Article

SOURCE DATA TRANSPARENT PROCESS

THE EMBO JOURNAL

Arabidopsis HEAT SHOCK FACTOR BINDING PROTEIN is required to limit meiotic crossovers and *HEI10* transcription

Juhyun Kim[1,†], Jihye Park[1,†], Heejin Kim[1], Namil Son[1], Eun-Jung Kim[1], Jaeil Kim[1], Dohwan Byun[1], Youngkyung Lee[1], Yeong Mi Park[1], Divyashree C Nageswaran[2], Pallas Kuo[2], Teresa Rose[3], Tuong Vi T Dang[1], Ildoo Hwang[1], Christophe Lambing[2,3], Ian R Henderson[2] & Kyuha Choi[1,*]

Abstract

The number of meiotic crossovers is tightly controlled and most depend on pro-crossover ZMM proteins, such as the E3 ligase HEI10. Despite the importance of HEI10 dosage for crossover formation, how *HEI10* transcription is controlled remains unexplored. In a forward genetic screen using a fluorescent crossover reporter in *Arabidopsis thaliana*, we identify heat shock factor binding protein (HSBP) as a repressor of *HEI10* transcription and crossover numbers. Using genome-wide crossover mapping and cytogenetics, we show that *hsbp* mutations or meiotic *HSBP* knockdowns increase ZMM-dependent crossovers toward the telomeres, mirroring the effects of *HEI10* overexpression. Through RNA sequencing, DNA methylome, and chromatin immunoprecipitation analysis, we reveal that HSBP is required to repress *HEI10* transcription by binding with heat shock factors (HSFs) at the *HEI10* promoter and maintaining DNA methylation over the *HEI10* 5′ untranslated region. Our findings provide insights into how the temperature response regulator HSBP restricts meiotic *HEI10* transcription and crossover number by attenuating HSF activity.

Keywords Crossover; HEI10; HSBP; HSF; meiosis
Subject Categories Chromatin, Transcription & Genomics; DNA Replication, Recombination & Repair; Plant Biology
DOI 10.15252/embj.2021109958 | Received 14 October 2021 | Revised 21 April 2022 | Accepted 27 April 2022 | Published online 7 June 2022
The EMBO Journal (2022) 41: e109958

Introduction

During meiosis, homologous chromosomes (homologs) undergo reciprocal DNA exchanges, called crossovers. Crossovers ensure the correct segregation of homologs during meiosis I and create new combinations of alleles in gametes (Villeneuve & Hillers, 2001; Hunter, 2015). Meiotic recombination is initiated by the formation of DNA double-strand breaks (DSBs) (Gray & Cohen, 2016). Numerous DSBs are formed, but only about 5% of DSBs are repaired as crossovers, and thus, the number of crossovers is limited to 1–3 per homolog (Mercier *et al*, 2015). Meiotic DSB ends are resected to generate 3′ single-stranded DNA ends that are then bound by recombinases DMC1 and RAD51 (Gray & Cohen, 2016). The resulting nucleoprotein complex then invades sister or non-sister chromatids to produce a displacement loop (D-loop) structure (Hunter, 2015; Gray & Cohen, 2016). Interhomolog D-loops are resolved into crossovers by the formation of double Holliday junctions (dHJs). Alternatively, D-loops are dissolved to produce non-crossovers (Hunter, 2015; Mercier *et al*, 2015).

Two crossover pathways are conserved across eukaryotes (Mercier *et al*, 2015). The class I pathway is responsible for approximately 85–90% of crossovers in Arabidopsis (*Arabidopsis thaliana*) (Mercier *et al*, 2015). Class I crossover formation is promoted by a group of ZMM proteins (ZIP4, SHOC1, PTD, MER3, MSH4, MSH5, and HEI10) and MutLγ (MLH1–MLH3) dHJ resolvases (Copenhaver *et al*, 2002; Higgins *et al*, 2004; Mercier *et al*, 2005, 2015; Chelysheva *et al*, 2012; Duroc *et al*, 2017; De Muyt *et al*, 2018). ZMM proteins stabilize interhomolog D-loops and protect them from anti-crossover helicases and facilitate the recruitment of MutLγ resolvases at crossover sites (Pyatnitskaya *et al*, 2019; Cannavo *et al*, 2020). Class I crossovers are subject to interference, which prevents the formation of another crossover nearby (Berchowitz & Copenhaver, 2010). Conversely, class II crossovers are non-interfering and formed by MUS81 (Berchowitz *et al*, 2007). In *Arabidopsis*, class II crossovers are restricted by anti-recombination proteins such as FANCM, RECQ4A, and RECQ4B that promote non-crossovers (Crismani *et al*, 2012; Girard *et al*, 2015; Séguéla-Arnaud *et al*, 2015).

One of the ZMM proteins required for class I crossover formation is the E3 ubiquitin/SUMO ligase HEI10 (Human enhance of

1 Department of Life Sciences, Pohang University of Science and Technology, Pohang, Korea
2 Department of Plant Sciences, University of Cambridge, Cambridge, UK
3 Department of Plant Sciences, Rothamsted Research, Harpenden, UK
*Corresponding author. Tel: +82 54 279 2361; E-mail: kyuha@postech.ac.kr
†These authors contributed equally to this work

invasion-10) (Chelysheva *et al*, 2012; Wang *et al*, 2012; De Muyt *et al*, 2014; Qiao *et al*, 2014). *Arabidopsis* HEI10 is loaded onto the meiotic chromosome axes as numerous foci during early prophase I, followed by their progressive reduction in numbers during pachytene, with only approximately 10–12 HEI10 foci remaining from late pachytene to diakinesis, marking crossover sites with MLH1 foci (Chelysheva *et al*, 2012; Morgan *et al*, 2021). HEI10 interacts with several ZMM proteins in rice and *Arabidopsis* (Li *et al*, 2018; Zhang *et al*, 2019; Nageswaran *et al*, 2021). The biochemical activity of HEI10 remains elusive in plants, although protein modifications and degradation play critical roles in meiosis (Reynolds *et al*, 2013; Qiao *et al*, 2014; Rao *et al*, 2017; Gao & Colaiácovo, 2018). Studies in *Arabidopsis* and mice have shown that HEI10 is a dosage-sensitive pro-crossover factor (Qiao *et al*, 2014; Ziolkowski *et al*, 2017; Serra *et al*, 2018). HEI10 foci dynamics are also likely associated with crossover interference and the effects of temperature on class I crossover formation (Lloyd *et al*, 2018; Modliszewski *et al*, 2018; Morgan *et al*, 2021). Despite the importance of *HEI10* expression in controlling crossover numbers, very little is known about the regulation of *HEI10* transcription during meiosis.

In a forward genetic screen using a fluorescent crossover reporter in *Arabidopsis*, here, we describe the identification of *HIGH CROSSOVER RATE2* (*HCR2*), which encodes HSBP (heat shock factor binding protein), as a repressor of crossover frequency. The *hcr2* mutant and meiosis-specific *HSBP* knockdown increased *HEI10* transcript levels, leading to more crossovers in distal euchromatic regions and lower interference. HSBP is associated with heat shock factors (HSFs) at the *HEI10* promoter and maintained DNA methylation over the *HEI10* 5′ untranslated region. Our work, thus, revealed how the conserved HSBP-HSF transcriptional module controls *HEI10* transcription and restricts class I crossovers during meiosis.

Results

A forward genetic screen identifies *hcr2* as a hypomorphic allele (*hsbp-3*) of *HSBP*

To identify new anti-crossover factors, we performed a forward genetic screen for mutants with an elevated crossover rate using ethyl methanesulfonate (EMS) mutagenesis and the fluorescent recombination reporter *420* in the *Arabidopsis* Columbia-0 (hereafter, Col) background (Fig 1A and Appendix Fig S1A–B) (Nageswaran *et al*, 2021). The *420* reporter system carries two fluorescent reporter transgenes located on the upper arm of chromosome 3 and allows high-throughput measurements of crossover frequency in individual plants (Melamed-Bessudo *et al*, 2005; Ziolkowski *et al*, 2015, 2017; Nageswaran *et al*, 2021). We isolated the high crossover rate (*hcr*) mutants *hcr1*, *hcr2*, *hcr3*, and *hcr4* (*t*-test, all $P < 4.21 \times 10^{-5}$) (Fig 1A and B and Appendix Table S1) (Nageswaran *et al*, 2021). We showed previously that *HCR1* encodes PROTEIN PHOSPHATASE X-1 (PPX1), which interacts with ZMM proteins and limits class I crossovers, whereas *hcr4* was a *fancm* mutant allele (Nageswaran *et al*, 2021). The genetic distance measured between the two *420* fluorescent reporters was 35 cM in *hcr2*, representing a significantly higher crossover frequency (*t*-test, $P = 1.32 \times 10^{-10}$) than the 20 cM in Col, or *hcr2*/+ heterozygotes (*t*-test, *HCR2* versus *hcr2*/+, $P = 0.629$), indicating that *hcr2* is a recessive mutation (Fig 1C and Appendix Table S2). We mapped the causal *hcr2* mutation using a BC_1F_2 population and bulk segregant sequencing (Fig 1C and Appendix Fig S1C and D, and Table S3) (Sun & Schneeberger, 2015; Nageswaran *et al*, 2021). *hcr2* (hereafter *hsbp-3*; see below) harbored an EMS-driven single substitution mutation (C-to-T) close to the donor splicing site between the fourth and fifth exons in At4g15802, which encodes heat shock factor binding protein (HSBP) (Fig 1D). HSBP is conserved across eukaryotes and represses transcription by binding to heat shock transcription factors (HSFs) (Appendix Fig S2A–C) (Satyal *et al*, 1998; Hsu *et al*, 2010). The fourth intron of *Arabidopsis HSBP* is of the conserved minor AT-AC intron splicing class (Fig 1D and Appendix Fig S2D) (Russell *et al*, 2006). The C-to-T substitution in *hsbp-3* resulted in aberrant shorter and longer *HSBP* splice variants that introduce premature stop codons, compared to Col transcripts (Figs 1E and EV1A and B). We found that *HSBP* transcripts and HSBP protein levels decreased to approximately 53 and 58%, respectively, of Col levels in *hsbp-3* buds (Figs 1E and F, and EV1B and C). The *hsbp-1* and *hsbp-2*, T-DNA insertion mutants, also showed reduced *HSBP* transcript levels (*hsbp-1*, 70%; *hsbp-2*, 9%) and HSBP protein levels (*hsbp-1*, 77%; *hsbp-2*, 17%) relative to Col, indicating that *hsbp* alleles are unlikely to be null mutants but instead accumulate HSBP to different levels (Figs 1E and F, and EV1B and C).

To confirm that *HCR2* is *HSBP*, we generated complementation lines by introducing the entire *HSBP* genomic region from Col into

Figure 1. The *hcr2* mutant is a weak *hsbp* allele.

A Representative images of seed fluorescence segregation in *420*/++ in wild type (Col) and *hcr2*. Scatterplots to the right show red (dsRed) and green (eGFP) fluorescence values in *420*/++ Col (top) and *hcr2* (bottom). Scale bars: 2 mm.

B *420* crossover frequencies (cM) in Col, *hcr1*, *hcr2*, *hcr3*, and *hcr4* mutants. $n \geq 7$ plants of biological replicates.

C As in (B), *420* crossover frequencies (cM) in Col, *hcr2*/*HCR2*, *hcr2*/*hcr2*, and individual *hcr2* BC_1F_2 plants. $n \geq 6$ plants of biological replicates.

D Schematic diagram of the *HSBP* locus and position of the *hcr2* (*hsbp-3*) substitution (red asterisk). Black boxes, exons; gray boxes, UTRs; introns, black lines. The conserved splicing sequence of AT-AC class introns is underlined. Primer positions for the RT–PCR and RT–qPCR analyses are indicated by arrows.

E End-point RT–PCR analysis of *HSBP* in Col, *hsbp-3*, *hsbp-2*, and *hsbp-1*. Hash and asterisk indicate aberrant long and short splicing variants of *HSBP* in *hsbp-3*, respectively. Image J was used to measure relative PCR band intensity for *hsbp-3* (53%), *hsbp-2* (9%), and *hsbp-1* (70%). *TUB2* was used as an internal control.

F As in (E), but showing immunoblot analysis of HSBP. *hsbp-3*, *hsbp-2* and *hsbp-1* accumulate about 58, 17, and 77% of HSBP levels, respectively. Coomassie-stained membrane was used as a loading control.

G As in (B), *420* crossover frequencies in Col, *hsbp-3*, and *hsbp-3* T_1 lines harboring the *HSBP* or *HSBP-myc* transgene. $n \geq 6$ plants of biological replicates.

H As in (B), *420* crossover frequencies (cM) in Col, *hsbp-3*, and *meiMIGS-HSBP* T_1 transgenic plants. $n \geq 6$ plants of biological replicates.

I As in (B), but showing *I3bc* crossover frequency (cM) in Col, *hsbp-3*, *hsbp-3*/*hsbp-2* F_1 hybrid, and *hspb-2* plants. $n \geq 5$ plants of biological replicates.

Data information: (E, F) Experiments were performed at least three times. (B, G, H) Red dots and horizontal lines indicate mean ± s.d. of cM values from individual plants (one-sided Welch's *t*-test). Black dots represent cM values of individual plants. (I) Colored dots represent cM values from individual plants.
Source data are available online for this figure.

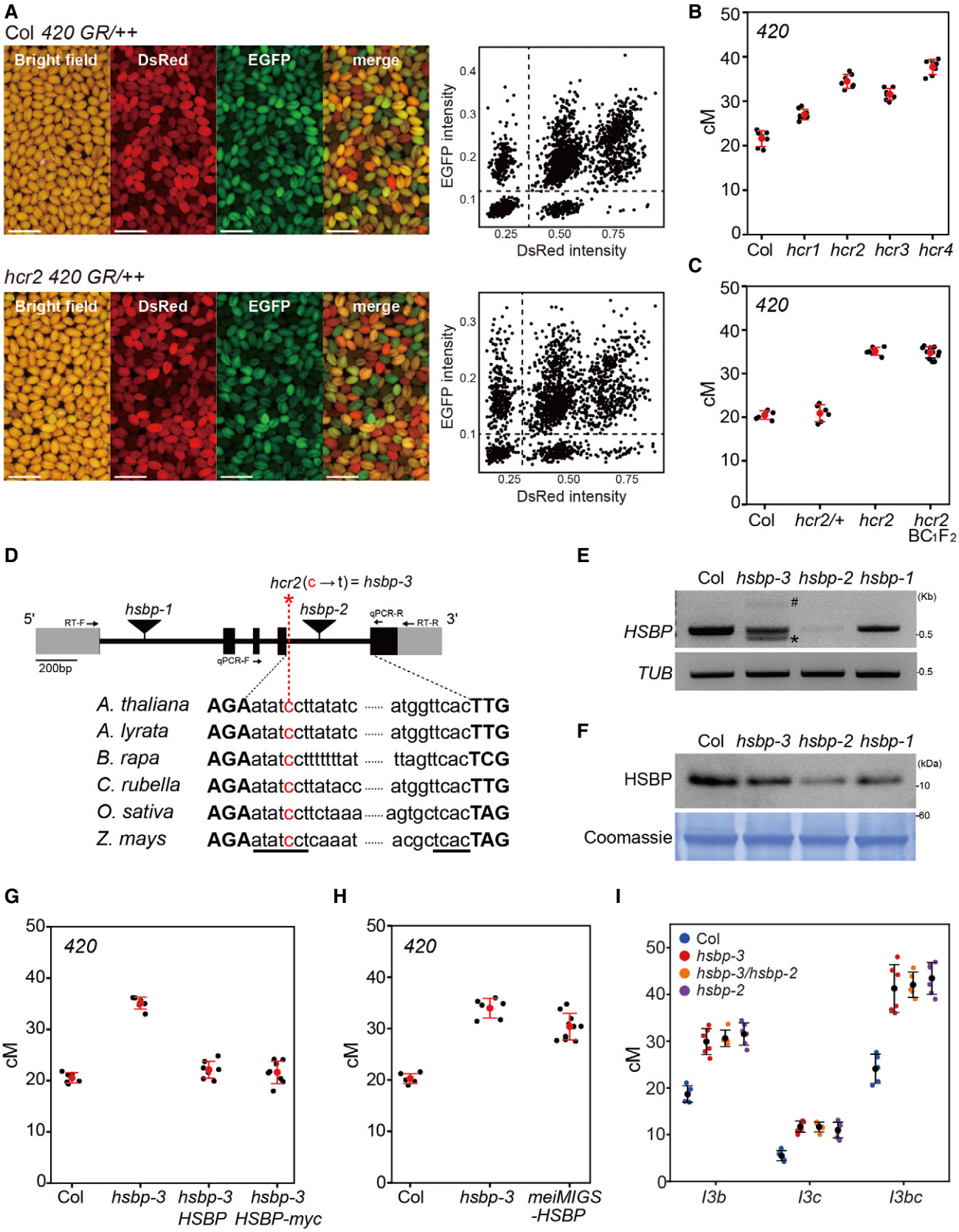
A
Col 420 GR/++
Bright field
DsRed
EGFP
merge
EGFP intensity
DsRed intensity
hcr2 420 GR/++
B
420
cM
Col hcr1 hcr2 hcr3 hcr4
C
Col hcr2/+ hcr2 hcr2 BC1F2
D
hcr2(c → t) = hsbp-3
hsbp-1
hsbp-2
5'
3'
RT-F
RT-R
qPCR-R
qPCR-F
200bp
A. thaliana AGAatatccttatatc atggttcacTTG
A. lyrata AGAatatccttatatc atggttcacTTG
B. rapa AGAatatccttttttat ttagttcacTCG
C. rubella AGAatatccttatacc atggttcacTTG
O. sativa AGAatatccttctaaa agtgctcacTAG
Z. mays AGAatatcctcaaat acgctcacTAG
E
Col hsbp-3 hsbp-2 hsbp-1
HSBP
TUB
(Kb)
F
HSBP
Coomassie
(kDa)
G
Col hsbp-3 hsbp-3 HSBP hsbp-3 HSBP-myc
H
Col hsbp-3 meiMIGS -HSBP
I
Col
hsbp-3
hsbp-3/hsbp-2
hsbp-2
I3b I3c I3bc

Figure 1.

the *420/++ hsbp-3* background via transformation (Fig 1G and Appendix Table S4). Primary (T_1) transgenic plants harboring genomic *HSBP* reduced the crossover frequency of the *hsbp-3* mutant to Col levels (*t*-test, *HSBP* $P = 0.192$, *HSBP-myc* $P = 0.436$) (Fig 1G and Appendix Table S4). We also specifically decreased *HSBP* transcript levels during meiosis using meiMIGS (meiosis-specific miRNA induced gene silencing) in the *420/++* background (Figs 1H and EV2A–E) (de Felippes *et al*, 2012; Nageswaran *et al*, 2021). These *meiMIGS*^{DMC1}*-HSBP* T_1 transgenic plants showed increased *420* crossover frequencies compared with Col plants (*t*-test, $P = 7.22 \times 10^{-8}$) (Fig 1H and Appendix Table S5). Importantly, *meiMIGS*^{DMC1}*-HSBP* T_2 plants had lower *HSBP* transcript levels that negatively correlated with *420* crossover frequencies ($r = -0.83$, $P = 1.28 \times 10^{-4}$) (Fig EV2E).

We then crossed the *420 hsbp-3* line with the *hsbp-2* T-DNA insertion allele to produce F_1 hybrid plants (*hsbp-3/hsbp-2*) for an allelism test (Fig 1D). The *hsbp-3/hsbp-2* F_1 hybrid plants exhibited increased *420* crossover frequencies compared to Col plants (*t*-test, $P = 1.03 \times 10^{-6}$) (Appendix Fig S3A). However, homozygous *hsbp*-2 F_2 seeds derived from these F_1 plants showed silencing of both fluorescent reporters in the seed coat, which led to altered segregation ratios (Appendix Fig S3B–D), possibly due to the role of HSBP in seed development (Fu *et al*, 2002; Hsu *et al*, 2010; Rana *et al*, 2012). We, therefore, used the three-color pollen FTL (fluorescence tagged line) *I3bc* to assess crossover frequencies in *hsbp-2* and *hsbp-3* using DeepTetrad (Lim *et al*, 2020) (Figs 1I and 2A). We allowed the *hsbp-3/hsbp-2* F_1 plants (*I3bc/+++*, *hsbp-3/hsbp-2*, *qrt1/QRT1*) to self-fertilize and measured crossover frequency in F_2 individuals (Fig 1I). Neither *hsbp-2* nor *hsbp-3* mutations led to silencing of the fluorescent reporters in the pollen grains (Appendix Fig S3E). Homozygous plants for *hsbp-3* or, *hsbp-2*, as well as *hsbp-3/hsbp-2* hybrid plants, showed increased crossover frequencies in *I3bc* compared with Col plants (*t*-test, all $P < 8.79 \times 10^{-5}$) but not between them (*t*-test, all $P > 0.305$) (Fig 1I and Appendix Table S6). Together, these results demonstrate that *HCR2* encodes HSBP.

hsbp-3 increases crossover frequency in euchromatic regions

We investigated the effect of *hsbp-3* on crossover frequency in other chromosomal regions. For this, we crossed *hsbp-3* with 22 seed fluorescent recombination reporters, CTLs (Col traffic lines) distributed across the genome, and measured sex-averaged *CTL* crossover frequency in individual F_2 plants (Fig 2A and Appendix Table S7) (Wu *et al*, 2015). Homozygous *hsbp-3* plants showed higher crossover frequency than Col plants in *CTLs* along euchromatic chromosome arms (*CTL1.17*, *CTL1.11*, *CTL1.13*, *CTL1.22*, *CTL2.8*, *CTL2.2*, *CTL2.7*, *CTL3.2*, *CTL3.6*, *CTL3.15*, *CTL4.7*, *CTL5.1*, *CTL5.2*, and *CTL5.14*) (*t*-test, all $P < 3.62 \times 10^{-4}$), which supports a role for HSBP in repressing crossover frequency outside of the *420* intervals (Fig 2B). However, crossover frequency decreased moderately (*CTL2.1*, *CTL3.9*, *CTL4.1*, *CTL5.5*) (*t*-test, all $P < 7.78 \times 10^{-3}$) or was unchanged (*CTL1.5*, *CTL3.8*) (*t*-test, *CTL1.5* $P = 0.847$, *CTL3.8* $P = 0.09$) in intervals spanning centromeres (Fig 2B). Indeed, we observed a strong negative correlation between the crossover increase in *hsbp-3* and the proximity of each *CTL* interval midpoint to the centromere ($r = -0.89$, $R^2 = 0.78$, $P = 3.145 \times 10^{-7}$) (Fig 2C). Consistently, the *meiMIGS* ^{DMC1}*-HSBP* line also exhibited higher crossover frequencies in the distal intervals *CTL1.13*, *CTL1.26*, and *CTL2.7* (*t*-test, all $P < 5.64 \times 10^{-4}$) but no difference in the centromeric interval *CTL1.5* (*t*-test, $P = 0.598$) (Fig 2D and Appendix Table S8).

HSBP limits crossovers in both male and female meiosis

We measured male- and female-specific crossover frequencies by reciprocally crossing *420/++ hsbp-3* with Col plants. *hsbp-3* significantly elevated *420* crossover frequencies during both male and female meiosis (*t*-test, all $P < 1.87 \times 10^{-7}$) (Fig 2E and Appendix Table S9), with a higher crossover frequency increase in female (*hsbp-3*, 283%) than male meiosis (*hspb-3*, 149%). This result indicated that HSBP restricts crossovers in females more strongly than in males. We further investigated the effects of *hsbp-3* on male crossover frequency using the pollen-specific FTLs *I1bc*, *I3bc*, and *I5ab* (Fig 2A). The *hsbp-3* mutant showed increased male crossover frequency in all tested FTL intervals (*t*-test, all $P < 2.35 \times 10^{-4}$) (Fig 2F and Appendix Table S10). In addition, multiple *meiMIGS-HSBP* T_1 plants with different meiosis-specific promoters (*DMC1*, *HEI10*, *ASY1*) displayed elevated *I3bc* crossover frequency in male meiosis, compared to Col plants (*t*-test, all $P < 8.38 \times 10^{-3}$) (Fig EV2F and Appendix Table S11).

hsbp-3 decreases crossover interference

The crossover interference ratio (IFR) is the ratio between an interval's map distance (cM) with and without an adjacent crossover,

Figure 2. *hsbp-3* and *meiMIGS-HSBP* increase crossover frequency and reduce interference strength.

A Seed and pollen FTL T-DNA intervals throughout the *Arabidopsis* genome used for crossover frequency measurements. Horizontal lines represent the intervals. Circles and triangles indicate *LAT52*- and *NapA*-driven FTL transgenes, respectively. The red asterisk indicates the chromosomal position of *hsbp-3*.
B Crossover frequencies of seed FTL/CTL lines in Col (blue) and *hsbp-3* (red). $n \geq 6$ plants of biological replicates.
C Correlation between FTL cM changes in *hsbp-3* and the midpoint of the FTL interval analyzed.
D As in (B), crossover frequencies of seed FTL in Col (blue) and *meiMIGS*^{DMC1}*-HSBP* (red). $n \geq 6$ plants of biological replicates.
E As in (B), *420* crossover frequencies (cM) in male and female meiosis for Col (blue) and *hsbp-3* (red). $n \geq 5$ plants of biological replicates.
F As in (B), crossover frequencies (cM) in pollen FTL *I1bc*, *I3bc*, and *I5ab* in Col and *hsbp-3*. $n \geq 5$ plants of biological replicates.
G Crossover interference ratios (IFRs) measured using FTL pollen tetrads in Col (blue) and *hsbp-3* (red). $n \geq 5$ plants of biological replicates.
H Double crossover (DCO) ratios detected in FTL pollen tetrads in Col (blue) and *hsbp-3* (red). The DCO ratio was calculated as (number of tetrads with more than two crossovers)/(total number of tetrads). $n \geq 5$ plants of biological replicates.

Data information: (B, D; E) Mean ± s.d. of cM values are indicated by black dots and horizontal lines (one-sided Welch's *t*-test). Blue and red dots indicate cM values from individual plants. (G) Mean ± s.d. of IFR values are indicated by black dots and horizontal lines. (H) Mean ± s.d. of DCO ratio values are indicated by black dots and horizontal lines (one-sided Welch's *t*-test).

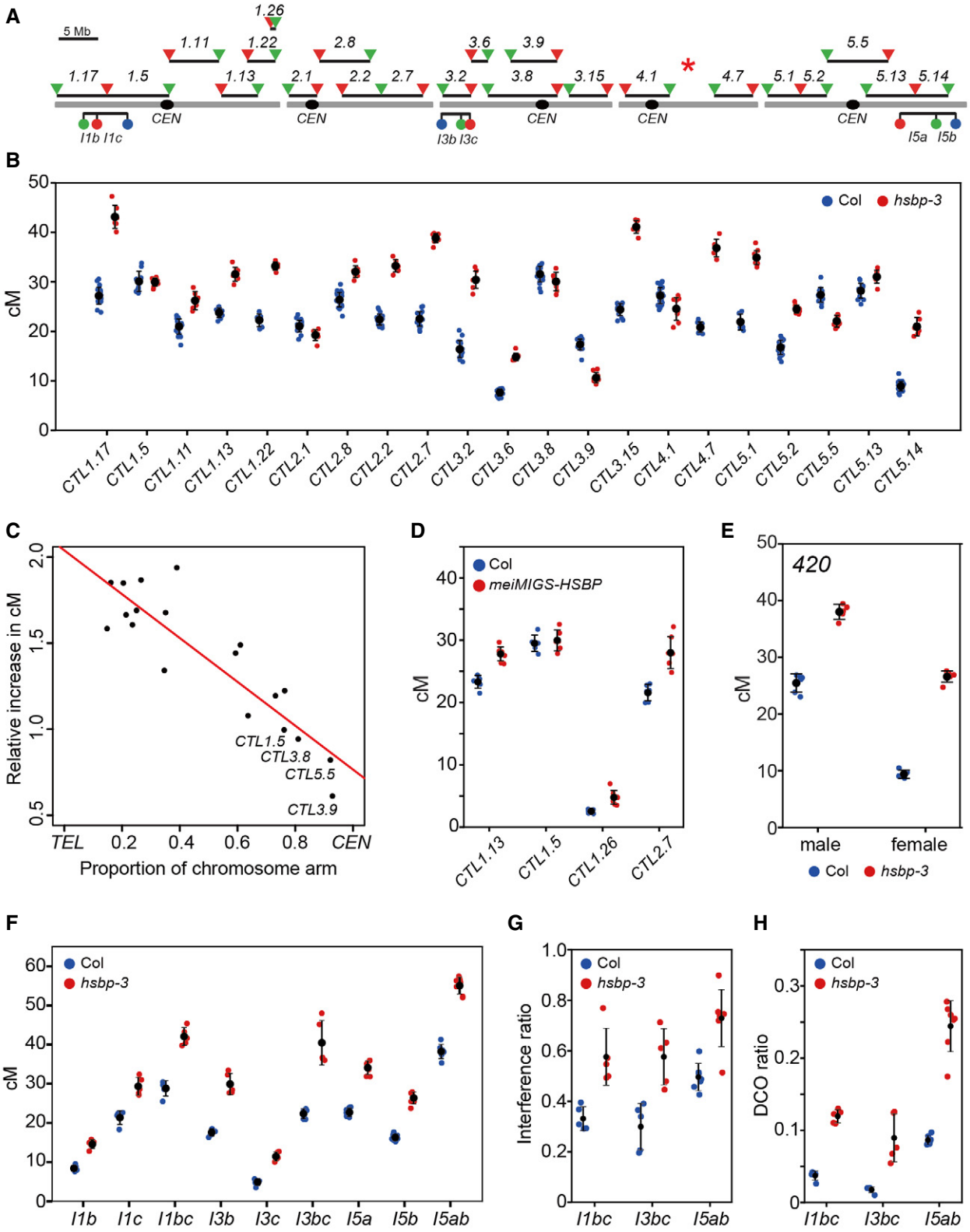
A
5 Mb
1.26
1.11
1.22
2.8
3.6
3.9
5.5
1.17
1.5
1.13
2.1
2.2
2.7
3.2
3.8
3.15
4.1
4.7
5.1
5.2
5.13
5.14
CEN
I1b I1c
I3b I3c
I5a I5b
B
cM
Col
hsbp-3
CTL1.17
CTL1.5
CTL1.11
CTL1.13
CTL1.22
CTL2.1
CTL2.8
CTL2.2
CTL2.7
CTL3.2
CTL3.6
CTL3.8
CTL3.9
CTL3.15
CTL4.1
CTL4.7
CTL5.1
CTL5.2
CTL5.5
CTL5.13
CTL5.14
C
Relative increase in cM
CTL1.5
CTL3.8
CTL5.5
CTL3.9
TEL
CEN
Proportion of chromosome arm
D
Col
meiMIGS-HSBP
CTL1.13
CTL1.5
CTL1.26
CTL2.7
E
420
male
female
F
I1b
I1c
I1bc
I3b
I3c
I3bc
I5a
I5b
I5ab
G
Interference ratio
I1bc
I3bc
I5ab
H
DCO ratio

Figure 2.

and it can be measured using three-color pollen FTLs (Francis *et al*, 2007; Berchowitz & Copenhaver, 2008; Lim *et al*, 2020). IFR values for FTLs *I1bc*, *I3bc*, and *I5ab* were significantly higher in *hsbp* compared to their values of Col (*t*-test, all $P < 5.55 \times 10^{-3}$), indicating that interference was weaker in *hsbp-3* relative to Col (Fig 2G and Appendix Table S10). Consistently, we detected more double crossovers within FTL intervals in *hsbp-3* compared with those in the Col (*t*-test, all $P < 8.02 \times 10^{-3}$) (Fig 2H). However, interference was still evident in *hsbp-3* with IFR values below 1, whereas class II anti-recombination mutants typically show no interference (IFR = 1) (Crismani *et al*, 2012; Girard *et al*, 2015; Séguéla-Arnaud *et al*, 2015). These findings indicate that HSBP is required for crossover interference.

Genetic analyses suggest that HSBP restricts class I crossovers

To understand how HSBP limits crossovers, we measured crossover frequency in double or triple mutants between *hsbp-3* and other recombination pathway mutants (Fig 3). We observed an additive increase in crossover frequency in both *420* and *CTL1.26* in the *fancm hsbp-3* double mutant compared with either single mutant (*t*-test, *fancm* $P = 0.012$, *hsbp-3* $P = 0.0134$) (Fig 3A and B, and Appendix Tables S12 and S13). Similarly, the *hcr1 hsbp-3* double mutant showed a higher crossover frequency in *CTL1.26* relative to the single mutants (*t*-test, *hcr1* $P = 4.97 \times 10^{-5}$, *hspb-3* $P = 1.85 \times 10^{-4}$) (Fig 3B and Appendix Table S13). Using the *I3bc* FTL, we detected an additive effect of *hsbp-3* on crossover frequency in *recq4a recq4b*, similar to *fancm* (*t*-test, *hsbp-3* $P = 1.30 \times 10^{-4}$, *recq4a recq4b* $P = 2.49 \times 10^{-3}$) (Fig 3C and Appendix Table S14). These results indicate that HSBP restricts crossover number independently of FANCM, RECQ4A/4B, and HCR1 (Fig 3A–C). Unlike *fancm* and *recq4a recq4b* mutants that restore the low fertility and bivalents of *zip4* mutants to Col levels by increasing class II crossovers (Crismani *et al*, 2012; Séguéla-Arnaud *et al*, 2015), *hsbp-3* restored neither *zip4* fertility (*zip4*, ~3.03 seeds/silique; *zip4 hsbp-3*, ~2.94 seeds/silique) (Wilcoxon test, $P = 0.11$) nor bivalents per cell of *zip4* (Wilcoxon test, $P = 0.17$) (Fig 3D–F and Appendix Tables S15 and S16). Furthermore, *420* crossover frequencies in the *hsbp-3 zip4* double mutant did not differ from that of *zip4* (*t*-test, $P = 0.977$), indicating that the elevated crossover frequency of *hsbp-3* requires ZIP4 activity (Fig 3A). Together, these genetic analyses indicate that HSBP represses class I crossover formation.

Meiotic *HSBP* knockdown elevates crossovers on chromosome arms in Col/Ler hybrids

Because *hsbp-3* elevated crossover frequency in Col inbred FTL intervals, we investigated the genome-wide effects of *hsbp-3* on crossover formation in Col/Ler hybrid plants. Accordingly, we mapped genomic crossover sites using genotyping by sequencing (GBS) of F_2 individuals derived from a cross between *420 meiMIGS-HSBP* in Col and Ler (Fig 4). We observed increased *420* crossover frequencies in *meiMIGS-HSBP* Col/Ler F_1 hybrids compared with those in Col/Ler F_1 plants (*t*-test, $P = 8.44 \times 10^{-11}$) (Fig 4A and B, and Appendix Table S17). We then performed GBS on 288 F_2 progeny from one *meiMIGS-HSBP* Col/Ler F_1 hybrid. Genome-wide crossover maps of *meiMIGS-HSBP* Col/Ler F_2 plants revealed more crossovers per individual F_2 plant (Wilcoxon test, $P = 2.2 \times 10^{-16}$) and per chromosome, compared with those in Col/Ler F_2 plants ($n = 240$) (Fig 4C and D, and Appendix Table S18). Most of the additional crossovers in *meiMIGS-HSBP* occurred within the chromosome arms toward the telomeres (Fig 4E and F), which was consistent with the increased crossover frequency seen in *hsbp-3* FTLs (Fig 2). Collectively, meiotic knockdown of *HSBP* increased crossovers on chromosome arms in both inbred and hybrid plants. We noticed that the *meiMIGS-HSBP* transgenic line might possess a T-DNA insertion-mediated chromosomal rearrangement, as evidenced by the suppression of crossovers around the pericentromere and the sharp increase in crossovers at the arms of chromosome 3 (Fig 4F). Therefore, we excluded chromosome 3 in the telomere and centromere analysis (Fig 4E).

hsbp and *meiMIGS-HSBP* increase *HEI10* transcription

Because HSBP interacts with HSF trimers and attenuates their transcriptional activity during the heat shock response (Satyal *et al*, 1998; Hsu *et al*, 2010), we performed transcriptome deep sequencing (RNA-seq) using *hsbp-3* and Col meiocyte-containing unopened buds (<1 mm) (Fig 5A). Among known meiotic genes, *HEI10* and *ASY1* transcript levels were significantly higher in *hsbp-3* compared with their levels in Col (Fig 5A). Increased *HEI10* transcript levels in *hsbp-3* were consistent with the higher crossover frequencies seen in the mutant (Figs 2 and 3) because HEI10 is a dosage-dependent pro-crossover factor in *Arabidopsis* (Ziolkowski *et al*, 2017; Serra *et al*, 2018). We confirmed higher *HEI10* and *ASY1* transcript levels in *hsbp-3*, *hsbp-2*, and *meiMIGS-HSBP* buds by RT–qPCR (*t*-test, all $P < 1.39 \times 10^{-2}$), while *DMC1*, *MLH1*, and *MUS81* transcript levels were comparable to those of Col (*t*-test, $P > 0.113$) (Appendix Fig S4A and C). To validate the effect of *hsbp-3* on *HEI10* transcription during meiosis, we purified male meiocytes and performed RT–qPCR analysis. We again observed elevated *HEI10* transcript levels in *hsbp-3* meiocytes compared with those in Col (*t*-test, $P = 1.15 \times 10^{-9}$) (Fig 5B). *HSBP* transcripts were also highly expressed in these purified meiocytes (*t*-test, $P = 2.93 \times 10^{-14}$) (Fig 5C) and meiotic buds (*t*-test, $P = 1.18 \times 10^{-12}$) (Appendix Fig S4B) compared with their expression in seedlings. Immunoblot analysis of HSBP indicated that HSBP abundance is also higher in buds than in seedlings (Fig EV1C) and reduced in *hsbp* and *meiMIGS-HSBP* buds (Fig EV2G). These results suggest that meiotic HSBP may limit crossover frequency by directly or indirectly repressing *HEI10* transcription.

hsbp-3 increases HEI10-dependent crossovers

To test the above hypothesis genetically, we generated a *hsbp-3 hei10* double mutant. *420* crossover frequencies were the same in the *hsbp-3 hei10* double mutant and in *hei10* (*t*-test, $P = 0.985$) (Fig 5D and Appendix Table S19), indicating that the increased crossovers in *hsbp-3* depend on HEI10 activity. *420* crossover frequencies also increased additively in Col and *hsbp-3* upon the introduction of a single copy of *HEI10-myc* transgene (*HEI10*, red) (Ziolkowski *et al*, 2017) (*t*-test, *hsbp-3* $P = 6.41 \times 10^{-4}$, *HEI10-myc* $P = 1.16 \times 10^{-5}$) (Fig 5D and Appendix Table S19). We confirmed the effect of *HEI10* copy number on increasing crossover frequency

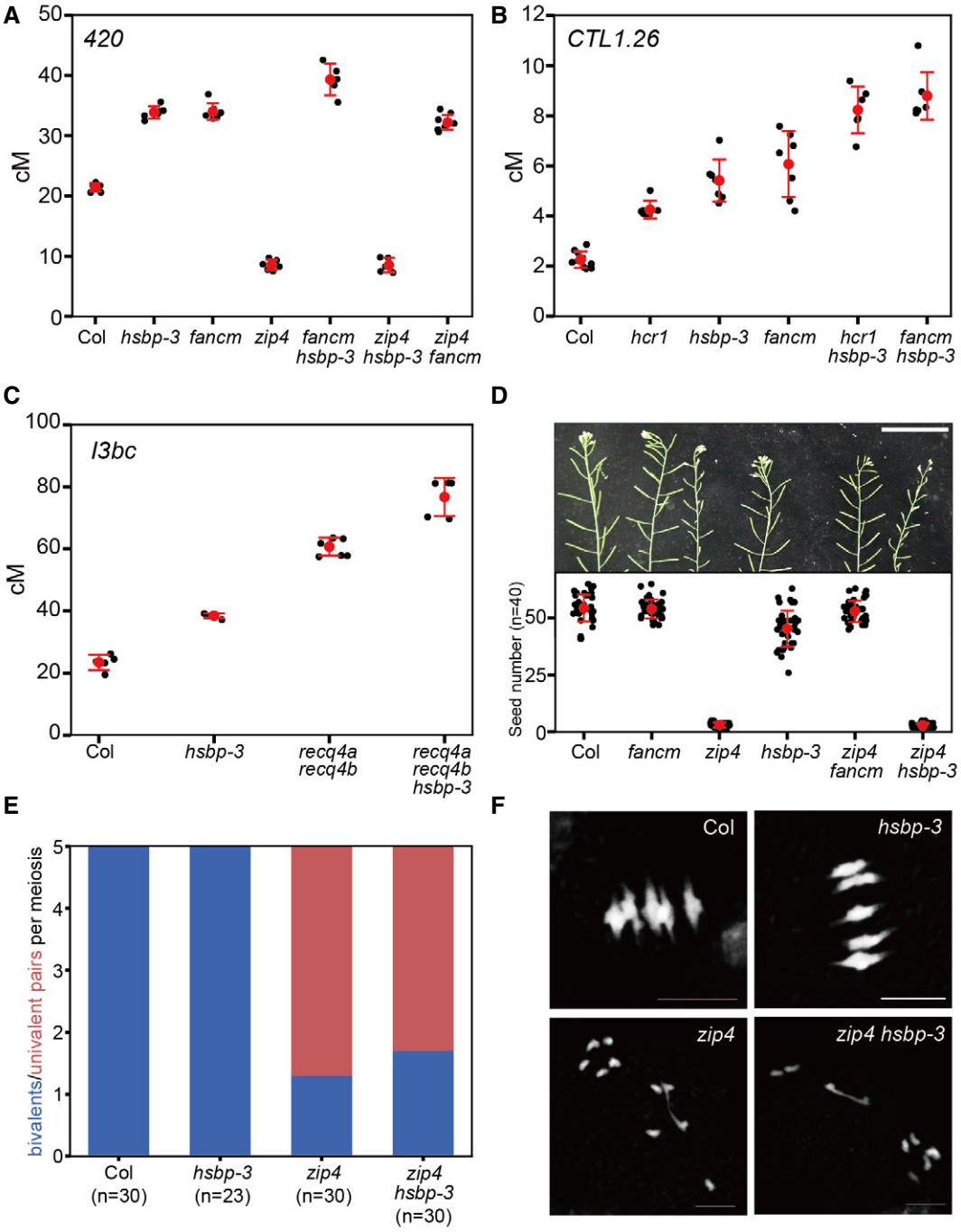

Figure 3. *hsbp-3* leads to an increase in ZMM-dependent crossovers.

A *420* crossover frequencies (cM) in Col, *hsbp-3*, *fancm*, *zip4*, *fancm hsbp-3*, *zip4 hsbp-3*, and *zip4 fancm*. $n \geq 5$ plants of biological replicates.

B As in (A), *CTL1.26* crossover frequencies (cM) in Col, *hcr1*, *hsbp-3*, *fancm*, *hcr1 hsbp-3*, and *fancm hsbp-3*. $n \geq 6$ plants of biological replicates.

C As in (A), *I3bc* crossover frequencies (cM) in Col, *hsbp-3*, *recq4a recq4b*, and *recq4a recq4b hsbp-3*. $n \geq 5$ plants of biological replicates.

D Representative silique images and average number of seeds per silique from Col, *fancm*, *zip4*, *hsbp-3*, *zip4 fancm*, and *zip4 hsbp-3* plants. Scale bar: 5 cm. Red dots and horizontal lines indicate mean ± s.d. of seed number from siliques. Black dots represent seed number from individual siliques. Significance between genotypes was assessed by Wilcoxon test. $n = 40$ siliques.

E Average number of bivalents (blue) and pairs of univalent (red) per male meiocyte from Col, *hsbp-3*, *zip4* and *zip4 hsbp-3*. The number of analyzed cells is indicated in parentheses. Significance between genotypes was assessed by Wilcoxon test.

F As in (E), but showing representative metaphase I chromosome spreads stained with DAPI. Scale bar, 10 μm. Images represent three biological replicates.

Data information: (A–C) Red dots and horizontal lines indicate mean ± s.d. of cM values (one-sided Welch's *t*-test). Black dots represent cM values of individual plants.

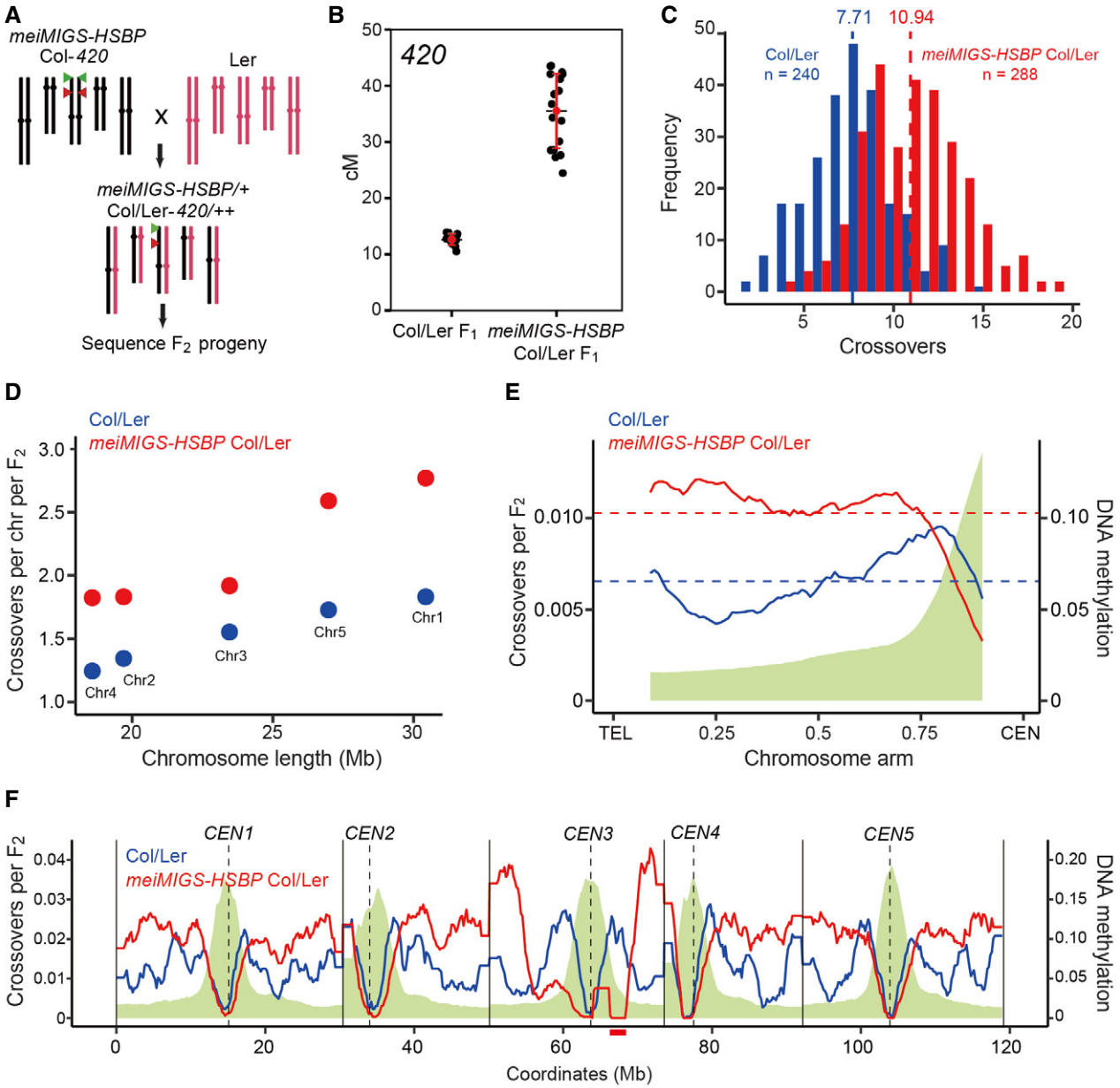

Figure 4. Genome-wide crossover maps in *meiMIGS-HSBP*.

A Schematic diagram of the crossing scheme between *meiMIGS-HSBP* Col-*420* (black) and Ler (red) to generate an F_2 population for genotyping by sequencing. Green and red triangles indicate the fluorescent reporters in the *420* background on chromosome 3.

B *420* crossover frequencies (in cM) in Col/Ler and *meiMIGS-HSBP* Col/Ler F_1 hybrids. Red dots and horizontal lines indicate mean ± s.d. of cM values (one-sided Welch's *t*-test). $n \geq 12$ plants of biological replicates.

C Distribution of crossover numbers per F_2 individual in Col/Ler (blue) and *meiMIGS-HSBP* Col/Ler (red). Vertical dashed lines indicate mean crossover numbers. Significance between genotypes was assessed by one-sided Welch's *t*-tests.

D Crossover numbers per chromosome in Col/Ler (blue) and *meiMIGS-HSBP* Col/Ler (red) F_2 populations.

E Normalized crossover frequencies along chromosome arms from the telomere (TEL) to the centromere (CEN) in Col/Ler (blue) and *meiMIGS-HSBP*/Ler F_2 populations (red). Crossover data for chromosome 3 were excluded due to a possible T-DNA-driven chromosome rearrangement. DNA methylation levels are shown in green. Horizontal dashed lines indicate mean values.

F As in (E), without TEL-CEN scaling. Vertical solid and dashed lines indicate telomeres and centromeres, respectively. The region of T-DNA-driven chromosome rearrangement in the pericentromere of chromosome 3 is shown as a solid red underline.

Data information: Significance between genotypes was assessed by one-sided Wilcoxon tests (D, E).

using a *HEI10-myc* transgenic line (one-way ANOVA test, all $P < 1.39 \times 10^{-8}$) (Fig 5E and Appendix Table S20) as previously reported (Ziolkowski *et al*, 2017). Varying *HEI10* transcript levels using the promoters of other meiotic genes (*ASY1*, *REC8*, *DMC1*) also increased *420* crossover frequencies to variable extents (*t*-test, all $P < 1.61 \times 10^{-5}$) (Fig 5E and Appendix Table S20).

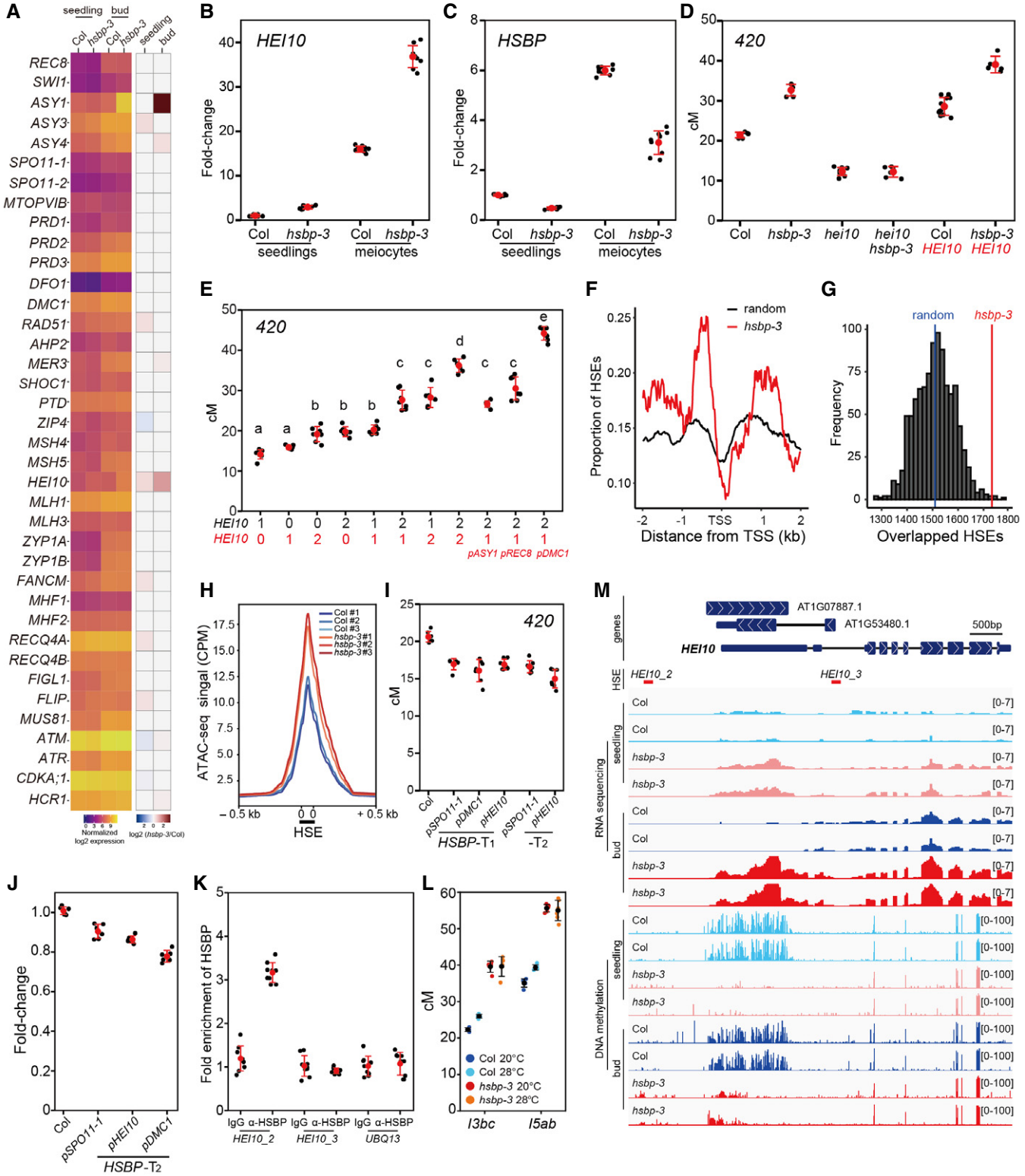

Figure 5.

Figure 5. HSBP represses *HEI10* transcription via HSF inhibition and DNA methylation.

A Heatmap representation of transcript levels for meiotic recombination genes in Col and *hsbp-3* seedlings and buds from RNA-seq data.

B *HEI10* transcript levels in Col and *hsbp-3* meiocytes, compared with seedlings by RT–qPCR. Experiments were performed at least three times. $n \geq 6$ two or three technical duplicates of three biological replicates.

C As in (C), *HSBP* transcript levels. $n \geq 6$ two or three technical duplicates of three biological replicates.

D *420* crossover frequencies in Col, *hei10*, *hsbp-3*, *hei10 hsbp-3*, *HEI10*, and *HEI10 hsbp-3*. *HEI10* (red), *HEI10-myc* transgene. $n \geq 6$ plants of biological replicates.

E As in (D), plants with different *HEI10* dosage and varying meiotic *HEI10* expression from the indicated promoters. Black numbers represent *HEI10* and the endogenous *HEI10* genotype (0, *hei10*; 1, *hei10*/*HEI10*; 2, *HEI10*/*HEI10*). Red numbers represent *HEI10* and *HEI10-myc* transgene copy number using *HEI10* or other meiotic gene promoters. One-way analysis of variance determined significant differences. $n \geq 6$ plants of biological replicates.

F Mean coverage of HSE peaks around the transcription start site (TSS) of upregulated genes ($n = 983$) in *hsbp-3* (red) and 1,000 sets of 983 randomly selected genes (black).

G As in (F), distribution of simulation frequencies (*y*-axis) and HSE numbers (x-axis) in upregulated genes in *hsbp-3* compared with 1,000 simulations of 983 randomly selected genes. Vertical blue line, mean number of the random HSE sets.

H Mean ATAC-seq signal around HSEs in Col and *hsbp-3* buds. The *y*-axis indicates mean CPM (counts per million mapped reads) of ATAC-seq.

I As in (D), *420* crossover frequencies in Col and transgenic plants expressing *HSBP* under the indicated promoters. $n \geq 6$ plants of biological replicates.

J As in (B), RT–qPCR analysis of *HEI10* in Col and meiotic *HSBP* transgenic plant (T_2) buds. $n \geq 6$ two or three technical duplicates of three biological replicates.

K HSBP ChIP–qPCR analysis at the *HEI10* promoter in buds. The *HEI10* primer positions are shown as red lines in (I). *UBQ13*, negative control. Experiments were performed three times. Data points (black) indicate three technical duplicates of three biological replicates. Red dots and horizontal lines indicate mean ± s.d. values (one-sided Welch's *t*-test).

L As in (D), but showing crossover frequency of *I3bc* and *I5ab* in Col and *hsbp-3* grown under optimal or high temperatures. Black dots and horizontal lines indicate mean ± s.d. of cM values from individual plants. Colored dots represent cM values of individuals. $n \geq 4$ plants of biological replicates.

M Integrative genomic viewer window showing the *HEI10* region of RNA-seq and BS-seq (DNA methylation) data in Col and *hsbp-3*.

Data information: (B, C, J) Data points (black) indicate two or three technical duplicates of three biological replicates. Red dots and horizontal lines indicate mean ± s.d. from duplicates (one-sided Welch's *t*-test). (D, E, I) Red dots and horizontal lines indicate mean ± s.d. of cM values from individual plants (one-sided Welch's *t*-test). Black dots represent cM values of individual plants.

HSBP directly represses *HEI10* transcription by binding and inhibiting HSFs

Because HSBP inhibits HSF activity by direct binding (Morimoto, 1998; Satyal *et al*, 1998), we investigated whether HSBP shares target genes with HSFs. We used published genome-wide HSE (heat stress element) maps from DNA affinity purification sequencing (DAP-seq) of HSFs (O'Malley *et al*, 2016). We plotted HSE peaks within 2-kb windows centered on transcription start sites of genes ($n = 983$) that are upregulated in *hsbp-3* (Fig 5F and G). We observed a significant enrichment of HSEs in the promoters of these upregulated genes compared with the mean coverage value of HSEs from 1,000 simulations with the same number ($n = 983$) of randomly selected genes (permutation test, $P < 2.2 \times 10^{-16}$) (Fig 5F and G), which suggests that HSBP and HSFs bind to a common set of genes.

To investigate if HSBP and HSFs control *HEI10* transcription *in vivo*, we performed protoplast transient transfection assays for HSFs, followed by RT–qPCR analysis of *HEI10* transcript levels. We selected *HSFA1a* and *HSFA7a* among the class A HSF activator family because they are highly expressed in meiotic buds and *HSFA7a* was induced in *hsbp-3* (Fig EV3A). Transient expression of *HSFA1a* or *HSFA7a* increased *HEI10* transcription (Fig EV3B and C). Importantly, HSBP inhibited HSF-mediated *HEI10* transcriptional activation when *HSBP* and *HSF* were co-transfected in protoplasts (Fig EV3B and C). To further examine the inhibition of HSF activity by HSBP, we performed ATAC-seq (assay of transposase accessible chromatin sequencing) in Col and *hsbp-3* buds to analyze DNA accessibility around 42,258 HSEs (Fig 5H) (O'Malley *et al*, 2016). *hsbp-3* showed elevated DNA accessibility around the HSEs, compared with Col, indicating that HSBP attenuates HSF DNA-binding and transcriptional activities (Fig 5H). To validate the inhibitory effect of HSBP on crossover frequency *in planta*, we generated transgenic *420*/++ plants that express *HSBP* additively using the *SPO11-1*, *DMC1*, or *HEI10* promoters. These transgenic T_1 and T_2 plants exhibited lower *420* crossover frequencies (*t*-test, all $P < 1.03 \times 10^{-5}$) and lower *HEI10* transcript levels (*t*-test, all $P < 2.78 \times 10^{-4}$) compared with Col plants (Fig 5I and J, and Appendix Table S21), suggesting that *HEI10* transcription is controlled by an HSF–HSBP transcriptional module whereby HSBP inhibits HSF activity during meiosis.

To examine if *HEI10* transcription is controlled directly by HSFs and HSBP, we performed chromatin immunoprecipitation, followed by qPCR analysis (ChIP–qPCR) for HSFA7a at the *HEI10* locus using a protoplast transient assay and HSF DAP-seq information (Fig EV3D and E) (O'Malley *et al*, 2016). We observed a significant enrichment of HSFA7a at one HSE within the *HEI10* promoter, thus defining an *in vivo* binding site of HSFA7a (*t*-test, *HEI10_2* $P = 1.17 \times 10^{-8}$) (Fig EV3E). Next, we performed ChIP–qPCR analysis for HSBP at the *HEI10* promoter in heat-treated seedlings (37°C, 4 h) and unopened buds (Figs 5K and EV3F). HSBP was enriched at the same HSE in the *HEI10* promoter in both buds and seedlings (*t*-test, buds, $P = 5.29 \times 10^{-12}$; seedlings, $P = 1.30 \times 10^{-9}$), which demonstrated that HSBP directly represses *HEI10* transcription. Exposure to high temperature (37°C) induced *HEI10* transcription even in Col seedlings (Fig EV3G), but the *hsbp-3* mutant seedlings displayed a de-repression of *HEI10* transcription under normal growth temperature (20°C), and this was exacerbated at high temperature (Fig EV3G). We also confirmed the high temperature and hydrogen peroxide (H_2O_2)-mediated translocation of HSBP from the cytosol to the nucleus, and the co-localization and co-immunoprecipitation of HSBP with HSF proteins in protoplasts (EV3H, I, K and L) (Hsu *et al*, 2010). These results indicate that HSBP represses *HEI10* transcription directly by binding and attenuating HSF function at the *HEI10* promoter.

HSBP is required for temperature-sensitive crossover control

High temperature increases class I crossovers compared to the optimal growth temperature of approximately 18°C in *Arabidopsis*

(Lloyd *et al*, 2018; Modliszewski *et al*, 2018). We, therefore, examined the effect of temperature (28°C versus 20°C) on crossover frequency in Col and *hsbp-3* using the FTLs *I3bc* and *I5ab*. We determined that high temperature increased crossover frequency moderately in *I3bc* (116.7%, *t*-test, $P = 3.24 \times 10^{-5}$) and *I5ab* (109.7%, *t*-test, $P = 2.61 \times 10^{-4}$) as previously reported (Lloyd *et al*, 2018; Modliszewski *et al*, 2018), whereas *hsbp-3* showed the same high crossover frequency at both temperatures (*I3bc*, 98.5%, *t*-test, $P = 0.95$; *I5ab*,100.8%, *t*-test, $P = 0.637$) (Fig 5L and Appendix Table S22). The effect of high temperature on crossovers was thus compromised in *hsbp-3*, indicating that HSBP contributes to the control of crossover formation in response to changes in temperature.

HSBP is required for 5′ UTR DNA methylation and transcriptional repression of *HEI10*

DNA cytosine methylation was reported to be enriched in the *HEI10* 5′ untranslated region (5′ UTR) in Col plants (Kawakatsu *et al*, 2016). To examine if HSBP controls *HEI10* transcription via DNA methylation, we performed bisulfite sequencing (BS-seq) using seedlings and unopened buds of Col and *hsbp-3* (Fig 5M and Appendix Fig S6). Intriguingly, *hsbp-3* led to a loss of DNA methylation at the *HEI10* 5′ UTR in both seedlings and buds compared with Col (Fig 5 M). We also found that the expression of genes associated with DNA demethylation pathways (*DEMETER, ROS1, DML2,* and *IDM1*) is induced in *hsbp-3* buds, which may contribute to the loss of methylation in a subset of genes including *HEI10* (Appendix Fig S6D–F). In Col tissues, DNA methylation levels at the *HEI10* 5′ UTR were higher in seedlings than in buds, suggesting that DNA methylation inhibits *HEI10* transcription and decreases during early meiosis. Consistent with the BS-seq results, the RNA-seq data demonstrated that *HEI10* transcript levels are 16-fold higher in Col meiocytes compared with seedlings and were also higher in *hsbp-3* seedlings and buds relative to Col (Fig 5M). To examine if HSBP is required for maintenance of the DNA methylation at the *HEI10* 5′ UTR, we performed McrBC–qPCR analysis with the cytosine methylation-sensitive endonuclease McrBC using seedlings and unopened buds for Col, *hsbp-3*, *hsbp-2*, and *meiMIGS-HSBP* (Appendix Fig S5A). McrBC–qPCR showed that both *hsbp-3* and *hsbp-2* had lower DNA methylation at the *HEI10* 5′ UTR in seedlings and buds compared with the DNA methylation in Col (Appendix Fig S5A). *meiMIGS-HSBP* plants showed a sharp reduction (34.4%) in DNA methylation at the *HEI10* 5′ UTR in buds but a modest reduction (7.78%) in seedlings (Appendix Figs S4A and S5A). Consistently, *meiMIGS-HSBP* did not increase *HEI10* transcript levels in seedlings to the same extent as *hsbp-3* or *hsbp-2* (Appendix Fig S4A).

To test the effect of DNA hypomethylation at the *HEI10* 5′ UTR on *HEI10* transcription and crossover frequency, we generated *420*/++ plants with epi-alleles at the *HEI10* 5′ UTR by crossing *420* to *met1* mutant (Appendix Fig S5B). Hypomethylated alleles at the *HEI10* 5′ UTR exhibited higher *420* crossover frequencies and *HEI10* transcription than Col (*t*-test, *420* all $P < 2.85 \times 10^{-5}$) (Appendix Fig S5C–E and Table S23). We also identified natural epigenetic variation at the *HEI10* 5′ UTR in *Arabidopsis* accession C24 (Kawakatsu *et al*, 2016), with a loss of DNA methylation that resulted in higher *HEI10* transcript levels in C24 seedlings and buds, relative to Col and Cvi (Appendix Fig S5F and G). Together, these results show that HSBP is required to maintain DNA hypermethylation at the *HEI10* 5′ UTR in both somatic tissue and meiotic buds, and natural variations likely contribute to changes in DNA methylation of *HEI10* 5′ UTR.

hsbp-3 shows higher MLH1 and HEI10 foci

We investigated meiosis cytologically using *Arabidopsis* male chromosome spreads (Fig 6). DAPI (4′,6-diamidino-2-phenylindole) staining of male meiocytes revealed no significant differences between the Col and *hsbp-3*, with normal synapsis, bivalent formation, and chromosome segregation (Fig 6A). The *hsbp-3* plants produced shorter siliques and had lower seed fertility (*t*-test, silique all $P < 1.31 \times 10^{-17}$, fertility all $P < 6.53 \times 10^{-6}$) (Fig 6B and C, and Appendix Tables S24 and S25), as previously described for other *hsbp* alleles (Hsu *et al*, 2010). Pollen viability of *hsbp-3* and *hsbp-2* did not differ from that of Col pollen, as evidenced by Alexander staining (Fig 6D and Appendix Table S26) (*t*-test, *hsbp-3* $P = 0.465$, *hsbp-2* $P = 0.334$), suggesting that reduced fertility in *hsbp-3* and *hsbp-2* mutants may result from seed abortion during embryogenesis.

We counted the number of RAD51 recombinase foci marking meiotic DSB sites along chromosome axes at the leptotene stage using co-immunostaining with ASY1, a marker of the chromosome axis (Fig 6E). *hsbp-3* and Col had comparable numbers of RAD51 foci (Wilcoxon test, $P = 0.588$) (Fig 6F and Appendix Table S27). We then investigated the number of MLH1 foci, which mark class I crossover sites (Fig 6G). Significantly more MLH1 foci accumulated

Figure 6. Increased MlH1 and HEI10 foci in *hsbp-3*.

A Representative images of meiocyte spreads stained with DAPI in Col and *hsbp-3* at the indicated meiotic stages. Scale bars: 10 μm.
B–D Silique lengths (B), seed numbers (C), and pollen viability (D) in Col, *hsbp-3*, and *hsbp-2*. Red dots and horizontal lines indicate mean ± s.d. of cM values (one-sided Welch's *t*-test). $n = 30$ siliques of biological replicates (B, C). $n = 10$ plants of biological replicates (D).
E Representative images of ASY1 (green) and RAD51 (red) immunostaining in Col and *hsbp-3*. Nuclei spreads were stained with DAPI (blue). Scale bars: 10 μm.
F Quantification of RAD51 foci numbers per cell in Col (blue) and *hsbp-3* (red). $n = 20$ cells of biological replicates.
G Representative images of MLH1 (red) immunostaining in Col, *hsbp-3*, *hsbp-2*, Col/Ler, and *meiMIGS-HSBP* Col/Ler. Nuclear DNA was stained with DAPI. Scale bar: 5 μm.
H Quantification of the number of MLH1 foci per cell is shown in (G). $n \geq 32$ cells of biological replicates.
I Representative images of HEI10 (red) and ASY1 (green) immunostaining in Col and *hsbp-3*. Scale bar: 2 μm.
J Quantification of the number of HEI10 foci per cell is shown in (I). $n \geq 21$ cells of biological replicates.
K Immunoblot analysis of HEI10 and HEI10-Myc in Col, *hsbp-3*, *HEI10-myc*, and *HEI10-myc* plants. Experiments were performed at least three times.
L Representative images of HSBP (green) immunostaining during meiosis. Nuclei spreads were stained with DAPI. Scale bars: 5 μm.

Data information: (F, H, J) Black dots and horizontal lines indicate mean ± s.d. of values (Wilcoxon test).
Source data are available online for this figure.

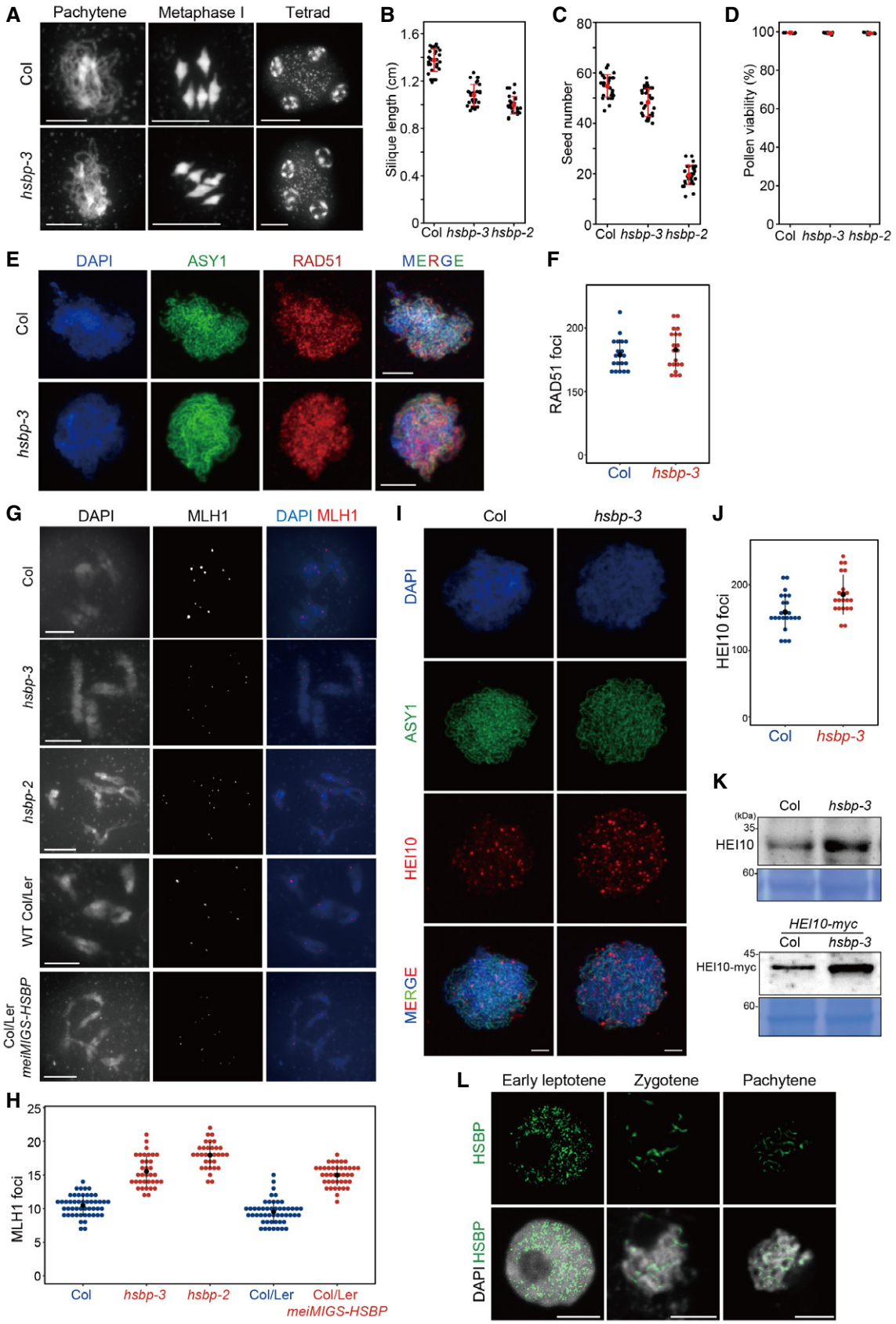

Figure 6.

in *hsbp-3, hsbp-2,* and *meiMIGS-HSBP* Col/Ler than in Col and Col/Ler plants (Wilcoxon test, *hsbp-3*, $P = 6.81 \times 10^{-14}$; *hsbp-2*, $P = 2.95 \times 10^{-14}$; *meiMIGS-HSBP*, $P = 4.89 \times 10^{-15}$) (Fig 6H and Appendix Table S28). We also counted the number of immunostained HEI10 foci per cell from the zygotene to the mid-pachytene stage (Fig 6I and J). *hsbp-3* showed more HEI10 foci per cell than Col (Wilcoxon test, $P = 4.45 \times 10^{-3}$) (Fig 6J and Appendix Table S29), which correlated with higher HEI10 and HEI10-myc abundance in the *hsbp-3* background, compared with control plants, as determined by immunoblot analysis (Fig 6K). This observation is consistent with increased *HEI10* transcription in *hsbp-3* and the genetic interactions of HSBP with meiotic recombination mutants (Figs 3 and 5). Finally, we determined the localization of HSBP during meiosis using immunostaining with an anti-HSBP antibody and *HSBPpro:HSBP-YFP* plants (Figs 6L and EV3J). We detected abundant HSBP proteins in the nucleus from leptotene to pachytene that overlap with DAPI signals in Col (Fig 6L), whereas HSBP abundance was low in *hsbp-3* and very low in *hsbp-2*, as expected from RT–PCR and immunoblot results (Fig 1E and F, and EV3J, and EV4).

Discussion

We demonstrate that the negative regulator of heat shock response HSBP directly represses *HEI10* transcription and restricts crossovers. HSBP forms hexamers that bind to the hydrophobic heptad repeat of HSFs, leading to their dissociation from active HSF trimers to inactive monomers, thereby attenuating HSF transcriptional and DNA-binding activities (Morimoto, 1998). In plants, transcript levels of heat shock-responsive genes increase in *hsbp* mutants and HSBP translocates from the cytosol to the nucleus at high temperatures (Fu *et al*, 2002; Hsu *et al*, 2010; Rana *et al*, 2012). Notably, *Arabidopsis* HSBP and its rice orthologs are highly expressed in reproductive tissues and are required for embryogenesis (Fu *et al*, 2002; Hsu *et al*, 2010; Rana *et al*, 2012). We determined that *Arabidopsis* HSBP is abundant in meiocytes and localizes to the nucleus during meiosis (Figs 5 and 6). Our identification of HSBP as a *HEI10* transcriptional repressor suggests a possible model for the control of *HEI10* expression, whereby HSFs activate *HEI10* transcription during early meiosis I, and the activity of HSFs is simultaneously or subsequently attenuated by HSBP, which may determine transcript levels of *HEI10* (Fig EV5A–C). We propose that a transcriptional module of HSFs and HSBP contributes to the regulation of meiotic *HEI10* transcription, and control of HEI10 protein level during early meiosis I (Chelysheva *et al*, 2012).

The cycle of HSF activity is dependent on high temperature through trimerization and nuclear translocation, DNA-binding, and post-translational modifications (Gomez-Pastor *et al*, 2018). In addition to high temperature, HSFs are activated by developmental signals, including reactive oxygen species (ROS) (Ahn & Thiele, 2003; Giesguth *et al*, 2015; Guo *et al*, 2016; Gomez-Pastor *et al*, 2018). In maize anthers, hypoxia facilitates somatic cells to differentiate as meiocytes (Kelliher & Walbot, 2012). Single-cell RNA-seq showed sharp and gradual expression patterns of meiotic recombination genes in maize; however, it remains largely unknown how developmental factors or signals control transcriptional changes of meiotic genes during plant meiosis (Nelms & Walbot, 2019). High *HSBP* expression levels and nuclear localization of HSBP observed here in meiocytes suggest that HSBP and HSFs may share meiotic signals such as ROS with other transcriptional regulators during transcriptional control of *HEI10* and other meiotic genes, including *ASY1*. Ambient temperatures outside of the optimal range may induce HSF activation and affect the developmental factors that increase class I crossovers in *Arabidopsis* (Choi *et al*, 2013; Lloyd *et al*, 2018; Modliszewski *et al*, 2018). In barley, a modest temperature shift leads to a higher number of interstitial chiasmata, indicating a conserved temperature effect on crossover formation (Higgins *et al*, 2012). However, high temperatures only modestly promoted class I crossovers (approximately 10–15%) in *Arabidopsis*, which is likely due to the inhibitory and buffering roles of HSBP on HSF activity for *HEI10* transcriptional control.

DNA methylation at the *HEI10* 5′ UTR was reduced in *hsbp-3*, which correlated with higher *HEI10* transcript levels. We found that HSBP is required to maintain DNA hypermethylation at the *HEI10* 5′ UTR; however, it remains unclear how HSBP maintains DNA hypermethylation specifically at the *HEI10* 5′ UTR. It is likely that transcription of *HEI10* contributes to reduce DNA methylation of the *HEI10* 5′ UTR during meiosis. *hsbp* might disrupt the cycle of HSF activity during meiosis, seed development, and responses to diverse environmental stresses. Therefore, *hspb* may cause the continuous production or accumulation of developmental and environmental stress signals such as protein misfolding and ROS, affecting DNA methylation via misregulation of genes involved in small RNA and DNA methylation pathways (Fig 5M and Appendix Figs S5 and S6F). A modest decrease in crossovers at pericentromeres and centromeres in *hsbp-3* and *meiMIGS-HSBP* is likely due to a slight increase in DNA methylation via upregulation of the genes involved in transposon-associated small RNA production and DNA methylation (Figs 2B and 4E, and Appendix Fig S6A–C and F). It is also worth noting that *hsbp* mutants may affect a newly identified epigenetic protein complex comprising a J-domain protein and HSP70 in plants (Ichino *et al*, 2021) because HSBP associates with HSP70 (Satyal *et al*, 1998). Determining whether and how HSBP, HSFs, HSPs, and temperature interact to modulate transcription and the epigenetic landscape in *Arabidopsis* accessions will be instrumental to our understanding of local adaptation and crossover change.

We determined that HSBP represses class I crossovers, adding to the previously described HCR1 and ZYP1 (Capilla-Pérez *et al*, 2021; France *et al*, 2021; Nageswaran *et al*, 2021). Genetic disruption of *HSBP* orthologs using genome editing or RNA interference may increase crossovers and accelerate breeding in crop species. Importantly, our findings shed light on how the evolutionarily conserved transcriptional regulators of HSFs and HSBP have been hitchhiked to control transcription during meiosis, epigenetic information, and crossover recombination in plants and other eukaryotes (Abane & Mezger, 2010).

Materials and Methods

Plant materials

The *Arabidopsis* (*Arabidopsis thaliana*) accession Col-0 was used as the wild type and grown in controlled growth rooms (20°C, 50–60% humidity, and 16-h-light/8-h-dark photoperiod). Seed and pollen

FTL lines were used as previously described (Melamed-Bessudo *et al*, 2005; Wu *et al*, 2015). The T-DNA insertion lines *hsbp-2* (SALK_093051) (Hsu *et al*, 2010), *zip4-2* (SALK_068052) (Chelysheva *et al*, 2012), and the *fancm-1* mutant (Crismani *et al*, 2012) were provided by the *Arabidopsis* Biological Resource Center (ABRC). Genotyping of *hcr2* was performed by PCR using oligonucleotides hcr2-geno F and R, followed by *Ssp*I (NEB, UK) restriction endonuclease digestion. Genotyping of *hsbp-2* was performed by PCR using primers hsbp-2 geno_F and R for Col and hsbp-2 geno_R and LBb1.3 for the T-DNA allele. The oligonucleotides used for genotyping, plasmid constructs, and experiments in this study are listed in Appendix Table S30.

Isolation and mapping of *hcr2*

The forward genetic screen and mapping of EMS-derived *hcr2* in the *420 GR*/++ hemizygous background were performed as described previously (Nageswaran *et al*, 2021). To map *hcr2*, the mutant *hcr2* in the *420* reporter background (*hcr2 420 GR/GR*) was backcrossed to Col. The resulting F_1 plants (*hcr2/HCR2*; *420 GR*/++) were allowed to self-fertilize to produce BC_1F_2 populations (Fig 1 and Appendix Fig S1). F_3 seeds from individual BC_1F_2 plants were harvested and used to measure the *420* crossover frequencies. Fifty F_2 plants with high crossover rates, as determined by *420* crossover frequencies in their F_3 seeds, were selected and their BC_1F_3 seeds were pooled. Nuclear genomic DNA (gDNA) of pooled F_3 seedlings was isolated and used to construct a DNA sequencing library as described (Nageswaran *et al*, 2021). The SHOREmap (v.3.0) pipeline was applied to map candidate mutations responsible for the *hcr2* (*hspb-3*) phenotype, as described (Nageswaran *et al*, 2021).

Genetic complementation of *hcr2* by a genomic copy of *HSBP*

A 3.8-kb *HSBP* gDNA fragment including the promoter (1.0-kb) and coding regions was PCR amplified using primers HSBP-genomic F and R (Appendix Table S30). For the *HSBP-myc* (*6x mycs*) transgenic line, the *HSBP* promoter and coding region without stop codon were PCR amplified using HSBP-genomic F and HSBP-myc R primers. The resulting PCR products were cloned into the binary vector pPZP211-*6x myc*, which harbors the *nopaline synthase* (*NOS*) terminator, as described (Choi *et al*, 2018). The pPZP211-*HSBP* and pPZP211-*HSBP-myc* constructs were electroporated into Agrobacterium (*Agrobacterium tumefaciens*) strain GV3101-pSOUP and transformed into *Arabidopsis 420*/++ F_1 Col plants by the floral dip method. T_1 plants were selected for kanamycin resistance, grown, and measured for *420* crossover frequencies.

Measurement of crossover frequency using fluorescent seed and pollen FTLs

The CellProfiler image analysis pipeline was used to measure crossover frequency (cM) by analyzing the number of fluorescent and non-fluorescent seeds from *FTL*/++ hemizygous plants (Carpenter *et al*, 2006; Ziolkowski *et al*, 2015). Crossover frequency (in cM) was calculated by counting green-alone fluorescent seeds (N_{Green}), red-alone fluorescent seeds (N_{Red}), and total seeds (N_{Total}) using the formula $cM = 100 \times \left(1 - [1 - 2(N_{Green} + N_{Red})/N_{Total}]^{1/2}\right)$ (Melamed-Bessudo *et al*, 2005; Ziolkowski *et al*, 2015). Welch's *t*-test was used to determine the significance of differences in crossover frequency between genotypes. Pollen tetrad FTL-based measurement of crossover frequency and interference ratio (IFR) were performed using DeepTetrad and pollen FTLs in the *qrt1* mutant background, as described (Berchowitz & Copenhaver, 2008; Lim *et al*, 2020).

Generation of *meiMIGS-HSBP* and meiotic *HSBP* transgenic plants

The vectors for meiosis-specific microRNA-mediated gene silencing (*meiMIGS*) transgenic plants were constructed using Golden Gate cloning, as described (Nageswaran *et al*, 2021). The *HSBP* coding sequence (At4g15802) was cloned into the Lv0 vector (pICH41331) following amplification using EJ-HSBP-F forward primers, which include the miR173 target sequence and EJ-HSBP-R reverse primers (Appendix Table S30). The Lv2 binary vector was electroporated into Agrobacterium strain GV3101-pSOUP and transformed into *Arabidopsis* via floral dipping. The promoters of meiotic genes were cloned into Lv0 vectors to drive *meiMIGS-HSBP* expression during meiosis. To generate transgenic plants that additively express *HSBP*, the Lv0 vectors with the *DMC1*, *SPO11-1*, or *HEI10* promoters were assembled individually into the Lv1 vector with *HSBP* Lv0 and pICH41421 terminator vector and subsequently assembled to Lv2 binary vectors.

RT–qPCR analysis

Total RNA was isolated using TRIzol reagent (Invitrogen) and used for reverse-transcriptase quantitative PCR using a reverse transcription kit (enzynomics, EZ405S). Total RNA of *Arabidopsis* male meiocytes was isolated from stage 9 floral buds by gently squeezing between a glass slide and coverslip as described (Walker *et al*, 2018). Quantitative PCR was performed using a CFX real-time PCR detection system (Bio-Rad). *TUB2 (TUBULIN BETA CHAIN2)* was used as a reference for normalization. RT–qPCRs were performed and analyzed for three biological replicates and three technical repeats per replicate.

HSBP protein purification and antibody generation

The coding sequence of *HSBP* (At4g15802) was amplified by PCR with pET-HSBP_F and pET-HSBP_R primers using the cDNA as template. The PCR product was cloned into the *Nde*I and *Xho*I restriction sites of pET30a (Novagen) to add a C-terminal 6x-his tag using the Gibson assembly cloning system. The resulting construct was transformed into *Escherichia coli* strain BL21 (DE3) RIL. Bacterial cells harboring the construct were grown in 1 L of LB medium containing kanamycin (50 mg/ml) and chloramphenicol (25 mg/ml) at 37°C. After the addition of 1.0-mM IPTG (Isopropyl-β-D-thiogalactoside), the culture was maintained at 18°C for 16 h for protein production. Bacterial cells were collected by centrifugation at 11,000 *g* for 15 min at 4°C and the pellet was resuspended in buffer A (40-mM Tris–HCl, pH 8.0). The cell pellet was disrupted by sonication and the cell debris was removed by centrifugation at 11,000 *g* for 30 min at 4°C. The lysate was bound to Ni-NTA agarose (QIAGEN) and the bound proteins were eluted with 300-mM imidazole in buffer A. Recombinant HSBP protein was purified by dialysis and used to produce the polyclonal antibody against HSBP by inoculating rabbits (GWVITEK, Korea).

Generation of genome-wide crossover maps by genotyping by sequencing (GBS)

Col/Ler and *meiMIGS-HSBP* Col/Ler F_2 individuals were grown on soil for 3 weeks. Genomic DNA (gDNA) from two to three adult leaves per plant was extracted by the CTAB method to prepare sequencing libraries as described (Ziolkowski *et al*, 2017; Serra *et al*, 2018; Nageswaran *et al*, 2021). Then, 150 ng gDNA from each F_2 plant was fragmented using dsDNA Shearase (Zymo Research) and used to generate one sequencing library per plant. The 96 barcoded libraries were pooled and subjected to paired-end 150-bp sequencing using an Illumina HiSeq X instrument (Macrogen, Korea). The TIGER pipeline was used to analyze the sequencing data and map crossovers as described (Nageswaran *et al*, 2021).

RNA sequencing

RNA extraction and library construction were performed as described (Choi *et al*, 2018). Briefly, 5 μg of total RNA was extracted from unopened floral buds (smaller than approximately 1 mm) and 10-day-old seedlings using TRIzol reagent (Invitrogen). A Ribo-Zero magnetic kit (MRZPL116, Epicentre) was used for rRNA depletion from total RNA. Then, 50 ng of rRNA-depleted RNA was used to construct sequencing libraries using a ScriptSeq v2 RNA-seq Library Preparation Kit (SSV21124, Epicentre). Twelve PCR cycles were used for amplification of the libraries, which were indexed using ScriptSeq Index PCR Primers (RSBC10948, Epicentre). Sequencing was performed on an Illumina HiSeq instrument (Macrogen, Korea). Adapter sequences were trimmed from the raw reads with Trim Galore (v. 0.6.6) with parameters -q 0 --stringency 3 --length 20. Trimmed reads were aligned to the TAIR10 reference genome using STAR (v. 2.7.3) (Dobin *et al*, 2013) with default parameters. The number of reads mapping to exons was calculated using featureCounts (v. 2.0.1) with default parameters (Liao *et al*, 2014). Differentially expressed genes (DEGs) were identified among meiosis-related genes (in-house list) with the R package *DESeq2* using a Benjamini–Hochberg adjusted *P*-value < 0.01 as cutoff (Love *et al*, 2014).

ATAC sequencing

The purification of nuclei and ATAC-seq library construction were performed as described (Maher *et al*, 2018). Briefly, 1 g of *Arabidopsis* unopened flower buds was ground in liquid nitrogen. The ground powder was resuspended in nuclei purification buffer (NPB, 20-mM MOPS, pH 7.0, 40-mM NaCl, 90-mM KCl, 2-mM EDTA, 0.5-mM spermidine, 0.2-mM spermine, 0.5-mM EGTA, 1× Roche Complete protease inhibitor cocktail). Nuclei were isolated by sucrose density gradient centrifugation. Approximately 100,000 nuclei were used for ATAC-seq library construction by measuring gDNA concentrations using a Qubit™ dsDNA BR Assay Kit (Thermo, Q32850). Tagmentation was performed using the Tagment DNA Enzyme and Buffer kit (Illumina, 20034210). Transposed DNA fragments were purified using AMPure XP beads (Beckman Coulter, A63881). After purification, transposed DNA was PCR amplified with 12 cycles using Next High-Fidelity 2×PCR Master Mix (NEB, M0541) with Nextera DNA CD Index primers. The indexed libraries were subjected to paired-end 50-bp sequencing using an Illumina HiSeq X instrument (Macrogen, Korea).

Genome-wide bisulfite sequencing (BS-seq) analysis

For BS-seq library construction, gDNA was isolated with the DNeasy Plant Mini Kit (Qiagen 69104, USA). The gDNA was fragmented by sonication using a Bioruptor (Diagenode, Belgium) to a mean size of approximately 250 bp, followed by blunt-ending, 3′-end dA addition, and adaptor ligation according to the manufacturer's instructions. The ligation products were used for bisulfite conversion using an EZ DNA Methylation-Gold kit (ZYMO). The different-sized fragments were separated and collected by electrophoresis on 2% Tris-acetate EDTA (TAE) agarose gels, followed by fragment purification (QIAquick Gel Extraction kit, Qiagen), PCR amplification, and cyclization. The DNA libraries were sequenced on a DNBseq platform (BGI, Hong Cong). BS-seq raw reads were aligned to the TAIR10 reference genome allowing one mismatch, and cytosine coverage was calculated using Bismark (v. 0.22.3). Identification of differentially methylated regions (DMRs) was performed as described (Williams & Gehring, 2017). All biological replicates were merged into one, and only the cytosines with a coverage of more than five reads were considered for further analysis. Cytosines with different methylation levels between *hsbp-3* and Col-0 (CG, 35%; CHG, 20%; CHH, 15%) were identified as differentially methylated cytosines (DMCs). Each 200-bp bin overlapping by 100 bp was assigned a "DMR score" calculated as:

$$(\#\text{hyper DMR} - \#\text{hypo DMR}) * \frac{\#\text{hyper DMR} + \#\text{hypo DMR}}{\#\text{cytosine}}$$

200-bp bins with a DMR score higher than 1.5 or lower than −1.5 were defined as hyperDMR or hyperDMR, respectively.

McrBC–qPCR analysis

gDNA was isolated using the DNeasy Plant Mini Kit (Qiagen 69104, USA). Then, 50 ng of gDNA was digested in NEBuffer2 with McrBC (NEB, M0272S) at 37°C for 4 h and inactivated at 65°C for 30 min. Digested DNA was used for quantitative PCR using a CFX real-time PCR detection system (Bio-Rad). gDNA in the same digestion reaction without McrBC treatment was used as a control. McrBC–qPCRs were performed and analyzed for three biological replicates and three technical repeats per replicate.

Immunocytological analysis of wild-type and *hsbp-3* meiocytes

Floral buds containing meiocytes were fixed in 3:1 (v/v) ethanol: acetic acid, and chromosome spreading was performed as described (Ross *et al*, 1996). The chromatin was stained with DAPI, and immunostaining of MLH1 was performed as described (Lambing *et al*, 2020). Co-immunostaining of ASY1, RAD51, and HEI10 was performed on chromosome spreads using Lipsol and fresh anthers, as described (Lambing *et al*, 2020). Images were captured using a DeltaVision Personal DV microscope (Applied Precision/GE Healthcare) equipped with a CDD CoolSNAP HQ2 camera (Photometrics). Image analyses were performed using softWoRx software version 5.5 (Applied Precision/GE Healthcare) and ImageJ. The following published antibodies were used: α-ASY1 (rat, 1:200 or 1:500 dilution), α-MLH1 (rabbit, 1:200 dilution), α-RAD51 (rabbit, 1:300 dilution), α-HEI10 (chicken, 1:1,000, a gift from Mathilde Grelon) and

α-HSBP (rabbit, 1:1,000 dilution) (Higgins *et al*, 2005; Sanchez-Moran *et al*, 2007; Chelysheva *et al*, 2010). Quantification of the number of MLH1 foci per meiotic cell and the number of RAD51 foci per cell associated with the axis protein ASY1 was performed manually. The number of HEI10 foci per cell was automatically counted using CellProfiler. A Wilcoxon test was used to assess significant differences for RAD51, MLH, and HEI10 foci counts between genotypes.

Arabidopsis protoplast transient transfection assays

Vectors for the transient transfection of *Arabidopsis* protoplasts were constructed using Golden Gate cloning. The full-length coding sequences of *HSBP* and *HSF*s were cloned into the Lv0 universal vector (pICH41331), as described (Nageswaran *et al*, 2021). Plasmid DNA transfection into protoplasts was performed as described (Nageswaran *et al*, 2021). To examine the effects of *HSF* and *HSBP* transient overexpression on *HEI10* transcription, 20 μg of plasmid DNA was transfected into 20×10^3 protoplasts and incubated at room temperature for 12 h, followed by incubation at 40°C for 1 h. Total RNA was isolated using TRIzol reagent (Invitrogen) for RT–qPCR analysis. For translocation of HSBP into the nucleus, colocalization, and co-immunoprecipitation of HSBP and HSF, 20 μg of total plasmid DNAs (*35Spro:HSF-GFP* and *35Spro:RFP-HSBP*) was co-transfected into protoplasts and incubated at room temperature for 12 h, followed by incubation at 40°C for 1 h. Fluorescence from transfected protoplasts was detected using a confocal microscope (LSM 800, Zeiss). Co-transfected protoplasts were used for co-immunoprecipitation and immunoblotting experiments, as described (Nageswaran *et al*, 2021).

Chromatin immunoprecipitation and quantitative PCR (ChIP–qPCR) analysis

HSF7a ChIP was performed using *Arabidopsis* protoplasts. Approximately 2×10^7 protoplasts were transfected with 400 μg of plasmid DNA (*35Spro:HSF7a-HA*) and incubated at room temperature for 6 h in constant low-light conditions (50 μmol m^{-2} s^{-1}), followed by incubation at 40°C for 1 h. Transfected protoplasts were crosslinked in 1% (w/v) formaldehyde for 10 min, then quenched with 0.125 M glycine for 5 min at room temperature. Crosslinked protoplasts were used for nuclei isolation, immunoprecipitation with anti-HA antibody (ab9110, Abcam), and DNA recovery as described (Choi *et al*, 2018). HSBP ChIP experiments were performed using 2 g of 10-day-old seedlings that were heat treated at 37°C for 4 h and unopened floral buds. Nuclei isolation, chromatin crosslinking, and recovery were performed as described (Choi *et al*, 2018). Briefly, chromatin was sheared using a Bioruptor pico instrument (Diagenode) for 10 min at high power alternating 30 s on/30 s off. Chromatin immunoprecipitation was performed using an α-HSBP antibody (10 μg), or normal IgG, and DNA purification was performed as described (Choi *et al*, 2018). Purified DNA was used for qPCR on a CFX real-time PCR detection system (Bio-Rad). All ChIP–qPCRs were performed and analyzed for three biological replicates and three technical repeats per replicate. The oligonucleotides used for the ChIP–qPCR are listed in Appendix Table S30.

Data availability

Sequencing data of F_2 individuals of *meiMIGS-HSBP* Col/Ler and Col/Ler have been deposited in the ArrayExpress database at EMBL-EBI (http://www.ebi.ac.uk/arrayexpress) under accession number E-MTAB-10168 (https://www.ebi.ac.uk/arrayexpress/experiments/E-MTAB-10168/), E-MTAB-10783 (https://www.ebi.ac.uk/arrayexpress/experiments/E-MTAB-10783/), and E-MTAB-11586 (https://www.ebi.ac.uk/arrayexpress/experiments/E-MTAB-11586/). RNA-seq, BS-seq, and ATAC-seq data for the Col and *hcr2* (*hsbp-3*) have been deposited in the ArrayExpress database at EMBL-EBI under accessions E-MTAB-10791 (https://www.ebi.ac.uk/arrayexpress/experiments/E-MTAB-10791/), E-MTAB-10657 (https://www.ebi.ac.uk/arrayexpress/experiments/E-MTAB-10657/), and E-MTAB-10790 (https://www.ebi.ac.uk/arrayexpress/experiments/E-MTAB-10790/).

Expanded View for this article is available online.

Acknowledgements

We thank Gregory Copenhaver (University of North Carolina), Avraham Levy (The Weizmann Institute), and Scott Poethig (University of Pennsylvania) for providing pollen and seed FTLs. We thank Raphael Mercier (Max Planck Institute, Cologne) for providing *fancm* and *recq4a recq4b* seeds. We thank Chris Franklin for providing ASY1 and RAD51 antibodies. We thank the Gurdon Institute for access to their microscopy facilities. We thank Charles Underwood (Max Planck Institute, Cologne), Yumi Kim (Johns Hopkins University), Mathilde Grelon (Institut National de la Recherche Agronomique, France), and Piotr Ziolkowski (Adam Mickiewicz University) for providing helpful comments. This work was funded by the Suh Kyungbae Foundation (SUHF) SUHF-17020079, Next-Generation BioGreen 21 Program PJ01337001, New Breeding Technologies Development Program PJ014795, Rural Development Administration, Basic Science Research Program through the National Research Foundation of Korea (NRF) funded by the Ministry of Education NRF-2020R1A2C2007763. CL research is funded by a BBSRC grant-aided support as part of the Institute Strategic Program Designing Future Wheat Grant (BB/P016855/1) and an Institutional Sponsorship Fund as part of the UKRI grant (BB/W510543/1). Work in the IRH group was supported by BBSRC grants BB/S006842/1, BB/S020012/1, and BB/V003984/1, European Research Council Consolidator Award ERC-2015-CoG-681987 'SynthHotSpot' and Marie Curie International Training Network 'COMREC'.

Author contributions

Juhyun Kim: Conceptualization; Data curation; Formal analysis; Investigation; Visualization; Methodology; Writing—original draft. **Jihye Park:** Data curation; Formal analysis; Validation; Investigation; Visualization; Methodology; Writing—original draft. **Heejin Kim:** Investigation; Visualization; Methodology; Writing—review & editing. **Namil Son:** Data curation; Software; Formal analysis; Validation; Visualization; Writing—review & editing. **Eun-Jung Kim:** Investigation; Methodology; Writing—review & editing. **Jaeil Kim:** Data curation; Formal analysis; Investigation; Visualization; Methodology; Writing—review & editing. **Dohwan Byun:** Data curation; Formal analysis; Validation; Investigation; Visualization; Methodology; Writing—review & editing. **Youngkyung Lee:** Investigation; Methodology; Writing—review & editing. **Yeong Mi Park:** Validation; Investigation; Methodology; Writing—review & editing. **Divyashree C Nageswaran:** Investigation; Methodology; Writing—review & editing. **Pallas Kuo:** Investigation; Methodology; Writing—review & editing. **Teresa Rose:** Investigation; Methodology. **Tuong Vi T Dang:** Methodology; Writing—review & editing. **Ildoo Hwang:** Supervision; Funding acquisition; Writing—review & editing. **Christophe Lambing:** Supervision; Funding acquisition; Investigation;

Visualization; Methodology; Writing—review & editing. **Ian R Henderson:** Formal analysis; Supervision; Funding acquisition; Writing—review & editing. **Kyuha Choi:** Conceptualization; Data curation; Formal analysis; Supervision; Funding acquisition; Investigation; Visualization; Methodology; Writing—original draft; Project administration; Writing—review & editing.

In addition to the CRediT author contributions listed above, the contributions in detail are:

JuK, JP, and KC designed experiments. JuK, JP, NS, DB, JaK, CL, IRH, and KC analyzed the data. JuK, JP, HK, NS, CL, EK, JaK, DB, YL, YMP, DCN, PK, TR, TVD, and KC conducted experiments. KC wrote the manuscript with assistance from JuK and JP. All authors reviewed the manuscript.

Disclosure and competing interests statement

The authors declare that they have no conflict of interest.

References

Abane R, Mezger V (2010) Roles of heat shock factors in gametogenesis and development. *FEBS J* 277: 4150–4172

Ahn SG, Thiele DJ (2003) Redox regulation of mammalian heat shock factor 1 is essential for Hsp gene activation and protection from stress. *Genes Dev* 17: 516–528

Berchowitz LE, Copenhaver GP (2008) Fluorescent *Arabidopsis* tetrads: a visual assay for quickly developing large crossover and crossover interference data sets. *Nat Protoc* 3: 41–50

Berchowitz LE, Copenhaver GP (2010) Genetic interference: don't stand so close to me. *Curr Genomics* 11: 91–102

Berchowitz LE, Francis KE, Bey AL, Copenhaver GP (2007) The role of AtMUS81 in interference-insensitive crossovers in *A. thaliana*. *PLoS Genet* 3: e132

Cannavo E, Sanchez A, Anand R, Ranjha L, Hugener J, Adam C, Acharya A, Weyland N, Aran-Guiu X, Charbonnier J-B *et al* (2020) Regulation of the MLH1–MLH3 endonuclease in meiosis. *Nature* 586: 618–622

Capilla-Pérez L, Durand S, Hurel A, Lian Q, Chambon A, Taochy C, Solier V, Grelon M, Mercier R (2021) The synaptonemal complex imposes crossover interference and heterochiasmy in *Arabidopsis*. *Proc Natl Acad Sci U S A* 118: 1–11

Carpenter AE, Jones TR, Lamprecht MR, Clarke C, Kang I, Friman O, Guertin DA, Chang J, Lindquist RA, Moffat J *et al* (2006) Cell Profiler: image analysis software for identifying and quantifying cell phenotypes. *Genome Biol* 7: R100

Chelysheva L, Grandont L, Vrielynck N, le Guin S, Mercier R, Grelon M (2010) An easy protocol for studying chromatin and recombination protein dynamics during *Arabidopsis thaliana* meiosis: immunodetection of cohesins, histones and MLH1. *Cytogenet Genome Res* 129: 143–153

Chelysheva L, Vezon D, Chambon A, Gendrot G, Pereira L, Lemhemdi A, Vrielynck N, Le Guin S, Novatchkova M, Grelon M (2012) The *Arabidopsis* HEI10 is a new ZMM protein related to Zip3. *PLoS Genet* 8: e1002799

Choi K, Zhao X, Kelly KA, Venn O, Higgins JD, Yelina NE, Hardcastle TJ, Ziolkowski PA, Copenhaver GP, Franklin FCH *et al* (2013) *Arabidopsis* meiotic crossover hot spots overlap with H2A.Z nucleosomes at gene promoters. *Nat Genet* 45: 1327–1336

Choi K, Zhao X, Tock AJAJ, Lambing C, Underwood CJCJ, Hardcastle TJTJ, Serra H, Kim JJ, Cho HSHS, Kim JJ *et al* (2018) Nucleosomes and DNA methylation shape meiotic DSB frequency in *Arabidopsis thaliana* transposons and gene regulatory regions. *Genome Res* 28: 532–546

Copenhaver GP, Housworth EA, Stahl FW (2002) Crossover interference in *Arabidopsis*. *Genetics* 160: 1631–1639

Crismani W, Girard C, Froger N, Pradillo M, Santos JL, Chelysheva L, Copenhaver GP, Horlow C, Mercier R (2012) FANCM limits meiotic crossovers. *Science* 336: 1588–1590

De Muyt A, Pyatnitskaya A, Andréani J, Ranjha L, Ramus C, Laureau R, Fernandez-Vega A, Holoch D, Girard E, Govin J *et al* (2018) A meiotic XPF–ERCC1-like complex recognizes joint molecule recombination intermediates to promote crossover formation. *Genes Dev* 32: 283–296

De Muyt A, Zhang L, Piolot T, Kleckner N, Espagne E, Zickler D (2014) E3 ligase Hei10: a multifaceted structure-based signaling molecule with roles within and beyond meiosis. *Genes Dev* 28: 1111–1123

Dobin A, Davis CA, Schlesinger F, Drenkow J, Zaleski C, Jha S, Batut P, Chaisson M, Gingeras TR (2013) STAR: ultrafast universal RNA-seq aligner. *Bioinformatics* 29: 15–21

Duroc Y, Kumar R, Ranjha L, Adam C, Guérois R, Md Muntaz K, Marsolier-Kergoat M-C, Dingli F, Laureau R, Loew D *et al* (2017) Concerted action of the MutLβ heterodimer and Mer3 helicase regulates the global extent of meiotic gene conversion. *eLife* 6: e21900

de Felippes FF, Wang J, Weigel D (2012) MIGS: miRNA-induced gene silencing. *Plant J* 70: 541–547

France MG, Enderle J, Röhrig S, Puchta H, Franklin FCH, Higgins JD (2021) ZYP1 is required for obligate cross-over formation and cross-over interference in *Arabidopsis*. *Proc Natl Acad Sci U S A* 118: 1–11

Francis KE, Lam SY, Harrison BD, Bey AL, Berchowitz LE, Copenhaver GP (2007) Pollen tetrad-based visual assay for meiotic recombination in *Arabidopsis*. *Proc Natl Acad Sci U S A* 104: 3913–3918

Fu S, Meeley R, Scanlon MJ (2002) Empty pericarp2 encodes a negative regulator of the heat shock response and is required for maize embryogenesis. *Plant Cell* 14: 3119–3132

Gao J, Colaiácovo MP (2018) Zipping and unzipping: protein modifications regulating synaptonemal complex dynamics. *Trends Genet* 34: 232–245

Giesguth M, Sahm A, Simon S, Dietz KJ (2015) Redox-dependent translocation of the heat shock transcription factor AtHSFA8 from the cytosol to the nucleus in *Arabidopsis thaliana*. *FEBS Lett* 589: 718–725

Girard C, Chelysheva L, Choinard S, Froger N, Macaisne N, Lehmemdi A, Mazel J, Crismani W, Mercier R (2015) AAA-ATPase FIDGETIN-LIKE 1 and helicase FANCM antagonize meiotic crossovers by distinct mechanisms. *PLoS Genet* 11: e1005369

Gomez-Pastor R, Burchfiel ET, Thiele DJ (2018) Regulation of heat shock transcription factors and their roles in physiology and disease. *Nat Rev Mol Cell Biol* 19: 4–19

Gray S, Cohen PE (2016) Control of meiotic crossovers: from double-strand break formation to designation. *Annu Rev Genet* 50: 175–210

Guo M, Liu JH, Ma X, Luo DX, Gong ZH, Lu MH (2016) The plant heat stress transcription factors (HSFS): Structure, regulation, and function in response to abiotic stresses. *Front Plant Sci* 7: 114

Higgins JD, Armstrong SJ, Franklin FCH, Jones GH (2004) The *Arabidopsis* MutS homolog AtMSH4 functions at an early step in recombination: evidence for two classes of recombination in *Arabidopsis*. *Genes Dev* 18: 2557–2570

Higgins JD, Perry RM, Barakate A, Ramsay L, Waugh R, Halpin C, Armstrong SJ, Franklin FCH (2012) Spatiotemporal asymmetry of the meiotic program underlies the predominantly distal distribution of meiotic crossovers in barley. *Plant Cell* 24: 4096–4109

Higgins JD, Sanchez-Moran E, Armstrong SJ, Jones GH, Franklin FCH (2005) The *Arabidopsis* synaptonemal complex protein ZYP1 is required for chromosome synapsis and normal fidelity of crossing over. *Genes Dev* 19: 2488–2500

Hsu SF, Lai HC, Jinn TL (2010) Cytosol-localized heat shock factor-binding protein, AtHSBP, functions as a negative regulator of heat shock response by translocation to the nucleus and is required for seed development in *Arabidopsis*. *Plant Physiol* 153: 773–784

Hunter N (2015) Meiotic recombination: the essence of heredity. *Cold Spring Harb Perspect Biol* 7: 1–36

Ichino L, Boone BA, Strauskulage L, Harris CJ, Kaur G, Gladstone MA, Tan M, Feng S, Jami-Alahmadi Y, Duttke SH *et al* (2021) MBD5 and MBD6 couple DNA methylation to gene silencing through the J-domain protein SILENZIO. *Science* 372: 1434–1439

Kawakatsu T, Huang S-S, Jupe F, Sasaki E, Schmitz RJ, Urich MA, Castanon R, Nery JR, Barragan C, He Y *et al* (2016) Epigenomic diversity in a global collection of *Arabidopsis thaliana* accessions. *Cell* 166: 492–505

Kelliher T, Walbot V (2012) Hypoxia triggers meiotic fate acquisition in maize. *Science* 337: 345–348

Lambing C, Kuo PC, Tock AJ, Topp SD, Henderson IR (2020) ASY1 acts as a dosage-dependent antagonist of telomere-led recombination and mediates crossover interference in *Arabidopsis*. *Proc Natl Acad Sci U S A* 24: 13647–13658

Li Y, Qin B, Shen Y, Zhang F, Liu C, You H, Du G, Tang D, Cheng Z (2018) HEIP1 regulates crossover formation during meiosis in rice. *Proc Natl Acad Sci U S A* 115: 10810–10815

Liao Y, Smyth GK, Shi W (2014) FeatureCounts: an efficient general purpose program for assigning sequence reads to genomic features. *Bioinformatics* 30: 923–930

Lim EC, Kim J, Park J, Kim EJ, Kim J, Park YM, Cho HS, Byun D, Henderson IR, Copenhaver GP *et al* (2020) DeepTetrad: high-throughput image analysis of meiotic tetrads by deep learning in *Arabidopsis thaliana*. *Plant J* 101: 473–483

Lloyd A, Morgan C, Franklin C, Bomblies K (2018) Plasticity of meiotic recombination rates in response to temperature in *Arabidopsis*. *Genetics* 208: 1409–1420

Love MI, Huber W, Anders S (2014) Moderated estimation of fold change and dispersion for RNA-seq data with DESeq2. *Genome Biol* 15: 550

Maher KA, Bajic M, Kajala K, Reynoso M, Pauluzzi G, West DA, Zumstein K, Woodhouse M, Bubb K, Dorrity MW *et al* (2018) Profiling of accessible chromatin regions across multiple plant species and cell types reveals common gene regulatory principles and new control modules. *Plant Cell* 30: 15–36

Melamed-Bessudo C, Yehuda E, Stuitje AR, Levy AA (2005) A new seed-based assay for meiotic recombination in *Arabidopsis thaliana*. *Plant J* 43: 458–466

Mercier R, Jolivet S, Vezon D, Huppe E, Chelysheva L, Giovanni M, Nogué F, Doutriaux M-P, Horlow C, Grelon M *et al* (2005) Two meiotic crossover classes cohabit in *Arabidopsis*: one is dependent on MER3, whereas the other one is not. *Curr Biol* 15: 692–701

Mercier R, Mézard C, Jenczewski E, Macaisne N, Grelon M (2015) The molecular biology of meiosis in plants. *Annu Rev Plant Biol* 66: 297–327

Modliszewski JL, Wang H, Albright AR, Lewis SM, Bennett AR, Huang J, Ma H, Wang Y, Copenhaver GP (2018) Elevated temperature increases meiotic crossover frequency via the interfering (Type I) pathway in *Arabidopsis thaliana*. *PLOS Genet* 14: e1007384

Morgan C, Fozard JA, Hartley M, Henderson IR, Bomblies K, Howard M (2021) Diffusion-mediated HEI10 coarsening can explain meiotic crossover positioning in *Arabidopsis*. *Nat Commun* 12: 4674

Morimoto RI (1998) Regulation of the heat shock transcriptional response: cross talk between a family of heat shock factors, molecular chaperones, and negative regulators. *Genes Dev* 12: 3788–3796

Nageswaran DC, Kim J, Lambing C, Kim J, Park J, Kim E-J, Cho HS, Kim H, Byun D, Park YM *et al* (2021) HIGH CROSSOVER RATE1 encodes PROTEIN PHOSPHATASE X1 and restricts meiotic crossovers in *Arabidopsis*. *Nat Plants* 7: 452–467

Nelms B, Walbot V (2019) Defining the developmental program leading to meiosis in maize. *Science* 364: 52–56

O'Malley RC, Huang SSC, Song L, Lewsey MG, Bartlett A, Nery JR, Galli M, Gallavotti A, Ecker JR (2016) Cistrome and epicistrome features shape the regulatory DNA landscape. *Cell* 165: 1280–1292

Pyatnitskaya A, Borde V, De Muyt A (2019) Crossing and zipping: molecular duties of the ZMM proteins in meiosis. *Chromosoma* 128: 181–198

Qiao H, Prasada Rao HBD, Yang YE, Fong JH, Cloutier JM, Deacon DC, Nagel KE, Swartz RK, Strong E, Holloway JK *et al* (2014) Antagonistic roles of ubiquitin ligase HEI10 and SUMO ligase RNF212 regulate meiotic recombination. *Nat Genet* 46: 194–199

Rana RM, Dong S, Tang H, Ahmad F, Zhang H (2012) Functional analysis of OsHSBP1 and OsHSBP2 revealed their involvement in the heat shock response in rice (Oryza sativa L.). *J Exp Bot* 63: 6003–6016

Rao HBDP, Qiao H, Bhatt SK, Bailey LRJ, Tran HD, Bourne SL, Qiu W, Deshpande A, Sharma AN, Beebout CJ *et al* (2017) A SUMO-ubiquitin relay recruits proteasomes to chromosome axes to regulate meiotic recombination. *Science* 355: 306–371

Reynolds A, Qiao H, Yang YE, Chen JK, Jackson N, Biswas K, Holloway JK, Baudat F, de Massy B, Wang J *et al* (2013) RNF212 is a dosage-sensitive regulator of crossing-over during mammalian meiosis. *Nat Genet* 45: 269–278

Ross KJ, Fransz P, Jones GH (1996) A light microscopic atlas of meiosis in *Arabidopsis thaliana*. *Chromosom Res* 4: 507–516

Russell AG, Charette JM, Spencer DF, Gray MW (2006) An early evolutionary origin for the minor spliceosome. *Nature* 443: 863–866

Sanchez-Moran E, Santos J-L, Jones GH, Franklin FCH (2007) ASY1 mediates AtDMC1-dependent interhomolog recombination during meiosis in *Arabidopsis*. *Genes Dev* 21: 2220–2233

Satyal SH, Chen D, Fox SG, Kramer JM, Morimoto RI (1998) Negative regulation of the heat shock transcriptional response by HSBP1. *Genes Dev* 12: 1962–1974

Séguéla-Arnaud M, Crismani W, Larchevêque C, Mazel J, Froger N, Choinard S, Lemhemdi A, Macaisne N, Van Leene J, Gevaert K *et al* (2015) Multiple mechanisms limit meiotic crossovers: TOP3α and two BLM homologs antagonize crossovers in parallel to FANCM. *Proc Natl Acad Sci U S A* 112: 4713–4718

Serra H, Lambing C, Griffin CH, Topp SD, Nageswaran DC, Underwood CJ, Ziolkowski PA, Séguéla-Arnaud M, Fernandes JB, Mercier R *et al* (2018) Massive crossover elevation via combination of HEI10 and recq4a recq4b during *Arabidopsis* meiosis. *Proc Natl Acad Sci U S A* 115: 2437–2442

Sun H, Schneeberger K (2015) Shoremap v3.0: fast and accurate identification of causal mutations from forward genetic screens. *Methods Mol Biol* 1284: 381–395

Villeneuve AM, Hillers KJ (2001) Whence meiosis? *Cell* 106: 647–650

Walker J, Gao H, Zhang J, Aldridge B, Vickers M, Higgins JD, Feng X (2018) Sexual-lineage-specific DNA methylation regulates meiosis in *Arabidopsis*. *Nat Genet* 50: 130–137

Wang K, Wang M, Tang D, Shen Y, Miao C, Hu Q, Lu T, Cheng Z (2012) The role of rice HEI10 in the formation of meiotic crossovers. *PLoS Genet* 8: e1002809

Williams BP, Gehring M (2017) Stable transgenerational epigenetic inheritance requires a DNA methylation-sensing circuit. *Nat Commun* 8: 2124

Wu G, Rossidivito G, Hu T, Berlyand Y, Poethig RS (2015) Traffic lines: new tools for genetic analysis in *Arabidopsis thaliana*. *Genetics* 200: 35–45

Zhang J, Wang C, Higgins JD, Kim YJ, Moon S, Jung KH, Qu S, Liang W (2019) A multiprotein complex regulates interference-sensitive crossover formation in rice. *Plant Physiol* 181: 221–235

Ziolkowski PA, Berchowitz LE, Lambing C, Yelina NE, Zhao X, Kelly KA, Choi K, Ziolkowska L, June V, Sanchez-Moran E *et al* (2015) Juxtaposition of heterozygous and homozygous regions causes reciprocal crossover remodelling via interference during *Arabidopsis* meiosis. *eLife* 4: e03708

Ziolkowski PA, Underwood CJ, Lambing C, Martinez-Garcia M, Lawrence EJ, Ziolkowska L, Griffin C, Choi K, Franklin FCH, Martienssen RA *et al* (2017) Natural variation and dosage of the HEI10 meiotic E3 ligase control *Arabidopsis* crossover recombination. *Genes Dev* 31: 306–317